NOV 0 1 1999 0830-L-02 NAS 1.29/3-2:99-10

NASA Tech Briefs

National Aeronautics and
Space Administration

Electronic Components and Circuits

Electronic Systems

Physical Sciences

Materials

Computer Programs

Mechanics

Machinery

Fabrication Technology

Mathematics and Information Sciences

Life Sciences

99-10 October 1999

2000-003538 (CFW) C

INTRODUCTION

Tech Briefs are short announcements of innovations originating from research and development activities of the National Aeronautics and Space Administration. They emphasize information considered likely to be transferable across industrial, regional, or disciplinary lines and are issued to encourage commercial application.

Availability of NASA Tech Briefs and TSPs

Requests for individual Tech Briefs or for Technical Support Packages (TSPs) announced herein should be addressed to

National Technology Transfer Center
Telephone No. **(800) 678-6882** or via World Wide Web at **www2.nttc.edu/leads/**

Please reference the control numbers appearing at the end of each Tech Brief. Information on NASA's Commercial Technology Team, its documents, and services is also available at the same facility or on the World Wide Web at **www.nctn.hq.nasa.gov**.

Commercial Technology Offices and Patent Counsels are located at NASA field centers to provide technology-transfer access to industrial users. Inquiries can be made by contacting NASA field centers and program offices listed below.

NASA Field Centers and Program Offices

Ames Research Center
Carolina Blake
(650) 604-0893 or
cblake@mail.arc.nasa.gov

Dryden Flight Research Center
Lee Duke
(805) 258-3802 or
lee.duke@dfrc.nasa.gov

Goddard Space Flight Center
George Alcorn
(301) 286-5810 or
galcorn@gsfc.nasa.gov

Jet Propulsion Laboratory
Merle McKenzie
(818) 354-2577 or
merle.mckenzie@ccmail.jpl.nasa.gov

Johnson Space Center
Hank Davis
(281) 483-0474 or
hdavis@gp101.jsc.nasa.gov

John F. Kennedy Space Center
Gale Allen
(407) 867-6626 or
galeallen-1@ksc.nasa.gov

Langley Research Center
Dr. Joseph S. Heyman
(804) 864-6006 or
j.s.heyman@larc.nasa.gov

Glenn Research Center
Larry Viterna
(216) 433-3484 or
cto@lerc.nasa.gov

George C. Marshall Space Flight Center
Sally Little
(256) 544-4266 or
sally.little@msfc.nasa.gov

John C. Stennis Space Center
Kirk Sharp
(228) 688-1929 or
ksharp@ssc.nasa.gov

NASA Program Offices
At NASA Headquarters there are seven major program offices that develop and oversee technology projects of potential interest to industry:

Carl Ray
Small Business Innovation Research Program (SBIR) & Small Business Technology Transfer Program (STTR)
(202) 358-4652 or
cray@mail.hq.nasa.gov

Dr. Robert Norwood
Office of Aeronautics and Space Transportation Technology (Code R)
(202) 358-2320 or
rnorwood@mail.hq.nasa.gov

John Mulcahy
Office of Space Flight (Code MP)
(202) 358-1401 or
jmulcahy@mail.hq.nasa.gov

Gerald Johnson
Office of Aeronautics (Code R)
(202) 358-4711 or
g_johnson@aeromail.hq.nasa.gov

Bill Smith
Office of Space Science (Code S)
(202) 358-2473 or
wsmith@sm.ms.ossa.hq.nasa.gov

Roger Crouch
Office of Microgravity Science Applications (Code U)
(202) 358-0689 or
rcrouch@hq.nasa.gov

Granville Paules
Office of Mission to Planet Earth (Code Y)
(202) 358-0706 or
gpaules@mtpe.hq.nasa.gov

NASA TechBriefs
National Aeronautics and Space Administration
October 1999
99-10

5 Electronic Components and Circuits
15 Electronic Systems
25 Physical Sciences
31 Materials
35 Computer Programs
39 Mechanics
43 Machinery
49 Fabrication Technology
53 Mathematics and Information Sciences

This document was prepared under the sponsorship of the National Aeronautics and Space Administration. Neither the United States Government nor any person acting on behalf of the United States Government assumes any liability resulting from the use of the information contained in this document, or warrants that such use will be free from privately owned rights.

BLANK PAGE

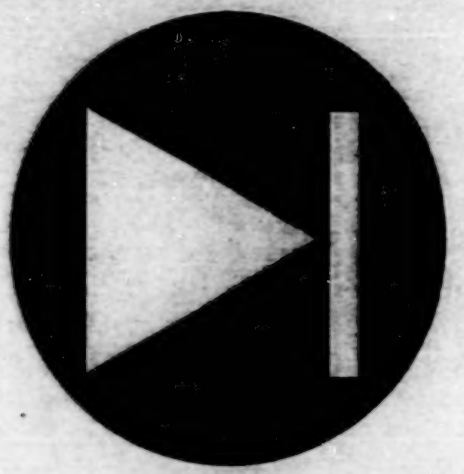

Electronic Components and Circuits

Hardware, Techniques, and Processes

7 Active-Pixel-Sensor ICs With Photosites in Substrates
8 GaN-Based Linear Array of Ultraviolet Detectors
9 Integrated Infrared- and Visible-Image Sensors
10 Inflatable Reflectarray Antennas
10 Filtering To Increase Effective Yields of Image Sensors
11 Frequency-Scanning Capaciflectors
12 Hybrid Imaging Technology
13 High-Speed Image Detectors With Subelectron Noise Floors
13 Improved Control of Charging Current for Ni/H Battery

BLANK PAGE

Active-Pixel-Sensor ICs With Photosites in Substrates

Heretofore, SOI CMOS has been considered unsuitable for APS circuits.

NASA's Jet Propulsion Laboratory, Pasadena, California

Focal-plane arrays of active-pixel sensors (photodetectors integrated with in-pixel readout transistors) would be designed and fabricated within the emerging technological discipline of silicon-on-insulator (SOI) complementary metal oxide/semiconductor (CMOS) integrated circuits (ICs), according to a proposal. SOI CMOS seems destined to supplant the more familiar bulk CMOS as the standard for fabrication of very-large-scale integrated (VLSI) circuits, during the next few years. Heretofore, it has been generally considered that functional APS circuits cannot be implemented in SOI CMOS because the layers of silicon for fabricating electronic devices on SOI wafers are so thin that optical absorbing volumes cannot be made large enough. In the proposed approach, photodetectors would be implemented within SOI silicon substrates in such a way as to obtain the desired functionality. Little or no departure from established SOI CMOS processing would be necessary. One disadvantage of SOI might be a tendency toward the floating-body effect, but it is possible to counteract this effect through appropriate design.

The figure depicts two of several proposed APS designs. The unique features of these designs and the advantages of implementing them in SOI CMOS rather than bulk CMOS include the following:

- The photodiode or photogate would incorporate part of the high-resistivity silicon substrate. This would impart a highly planar character to the device structure; the planar character would, in turn, prevent field-assisted increase in dark current (including dark current attributable to ionizing radiation.)
- The high resistivity of the substrate would make for a large depletion width, with consequent high quantum efficiency and thus high optical collection efficiency.
- Because the size of the photosite would be much larger than the minimum under design rules, the photosite could be fabricated along with other substructures by standard SOI fabrication techniques.
- The capacitance of the sensing node would be lower because the substrate capacitance would be lower. Lower sensing-node capacitance would translate to higher conversion gain and lower noise, and thus the ability to detect light at lower levels.

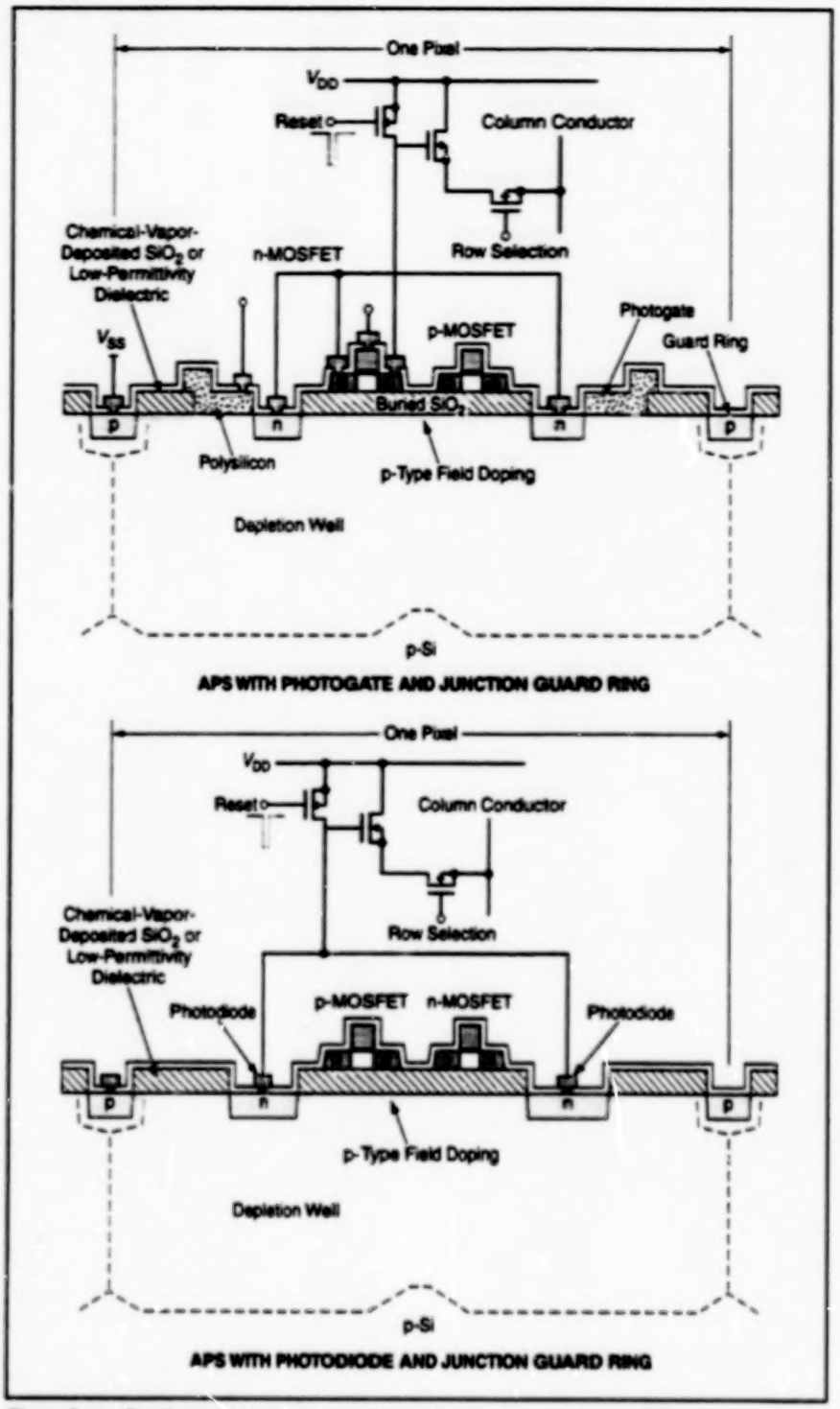

These Cross Sections (not to scale) represent unit cells of two of several APS designs proposed to be implemented in SOI CMOS.

- Complementary transistors would be placed in each pixel to obtain high dynamic range. A metal oxide semiconductor field-effect-transistor with p doping (p-MOSFET) would be incorporated for use as a reset gate that would enable reset all the way to the power-supply voltage (V_{DD}). It is not possible to incorporate such a structure into an APS in bulk CMOS without adversely affecting the pixel size and increasing the potential for latch-up, but it is possible in SOI

CMOS because SOI transistors are formed in isolated islands.

- Cross-talk would be reduced because parasitic capacitances would be lower and because of the isolation of individual transistors.
- In the absence of substrate coupling, timing patterns could be changed to enable the simultaneous operation of analog and digital subcircuits. The change in timing patterns would enable operation at higher speeds.
- Photodetectors, in-pixel circuitry, and peripheral circuitry would all exhibit greater radiation hardness because silicon layers would be thinner and because of the prevention of field-assisted increase in dark current mentioned above. Furthermore, the isolation of transistors would afford immunity to latch-up.

This work was done by Bedabrata Pain of Caltech for **NASA's Jet Propulsion Laboratory**. *Further information is contained in a TSP [see page 1].*
NPO-20534

GaN-Based Linear Array of Ultraviolet Detectors

This is a solar-blind array that can operate at room temperature.

Goddard Space Flight Center, Greenbelt, Maryland

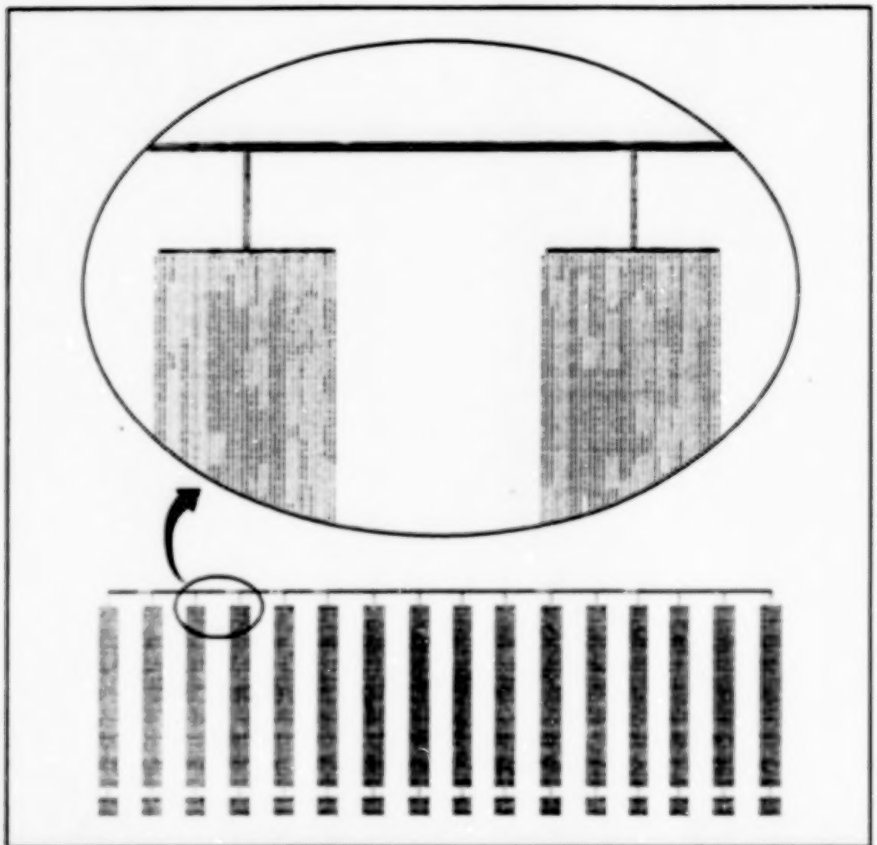

Figure 1. The Array Contains 16 Elements, each having an interdigitated metal/semiconductor structure with 20 fingers coming in from each end. The fingers are spaced at intervals of 4 μm. Each finger is 2 μm wide and 500 μm long.

A recently developed gallium nitride-based linear array of ultraviolet detectors is blind to most of the visible spectrum, with a cutoff wavelength of 370 nm. This device is a prototype of GaN detector arrays for ultraviolet-light imaging in the presence of significant visible radiation, without need for extensive baffling to suppress stray light or for costly filters to block visible light. The volume, weight, and power consumption of this GaN detector array is an order of magnitude below those of comparable photomultiplier tubes and microchannel plates now used to detect ultraviolet light. This GaN detector array also operates at lower voltage. Moreover, GaN is rugged, and the fabrication of detectors from GaN is relatively easy.

The prototype device — a 1 × 16 array — was fabricated by a conventional lift-off technique. Each detector element comprises a metal/semiconductor/metal interdigitated structure (see Figure 1). The overall area of the array is 4 mm^2. Semi-insulating GaN was used to obtain low dark current. The metal digits and connecting lines were formed in a Ti/Al/Au multilayer, which was used to ensure good ohmic contact.

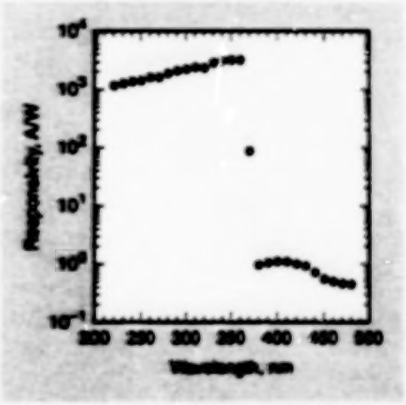

Figure 2. The Responsivity of One Detector Element was measured during operation at a potential under 10 V. Note the sharp cutoff at the wavelength of 370 nm.

Figure 2 shows the measured responsivity of one detector element. This detector element was found to have a responsivity of 3.1 ± 0.3 A/W at a wavelength of 365 nm, a response time of 0.5 ± 0.2 ms, and a dark current of 5×10^{-11} A; as of the time of submission of the information for this article, these performance figures were the best yet reported for GaN ultraviolet detectors.

There are numerous potential industrial, medical, and scientific-research applications for GaN detector arrays like this one. For example, because of their solar-blind nature, such arrays would be well suited for geophysical observation. They could also be used to detect ultraviolet light in hot environments and to detect ultraviolet emissions from flames and rocket exhausts.

This work was done by Zhenchun Huang, David Brent Mott, and Peter K. Shu of **Goddard Space Flight Center**. *No further documentation is available.*
GSC-13828

Integrated Infrared- and Visible-Image Sensors

It would not be necessary to split optical paths.

NASA's Jet Propulsion Laboratory, Pasadena, California

Integrated circuits capable of sensing both infrared and visible images have been proposed. Until now, the usual practice for simultaneous imaging at both infrared and visible wavelengths in the same camera has involved splitting of the optical path into an infrared and a visible branch, each containing a separate image sensor optimized for its wavelength range. In contrast, each of the proposed image sensors would include pixel detectors for both wavelength ranges, and sensors could be designed to operate with or without splitting of optical paths.

The figure illustrates five alternative design concepts for the proposed image sensors. In the first and second concepts, the infrared- and visible-light pixel detectors would be segregated into adjacent subimage areas, necessitating splitting of the optical path. The first concept calls for enlargement of the silicon integrated-circuit multiplexer chip of a traditional infrared image sensor to accommodate a visible-light image sensor on the additional area. The second concept is similar to the first one, except that the visible-light detectors would be implemented in a hybrid structure. The visible-readout portion of the multiplexer circuitry could be similar to the infrared-readout portion, or it could be designed as a photoelectron-counting circuit.

The third, fourth, and fifth concepts do not entail splitting of the optical path. According to the third concept, the visible and infrared pixel detectors would be interspersed throughout the same image area. The visible-image detectors could be of the complementary metal oxide/semiconductor (CMOS) active-pixel-sensor (APS) type. The infrared detectors could be of the thermopile or bolometer type. CMOS readout circuitry would be used for both sensors. The number of infrared pixels need not equal the number of visible pixels. The interspersion of infrared and visible pixels could be in any of a variety of patterns, depending on the requirements for spatial resolution in the infrared and visible images.

The fourth concept calls for stacking of a monolithic visible-image sensor on top of a monolithic infrared-image sensor. The visible-image sensor would have to be made of silicon, because the infrared light could pass through a silicon-based sensor to the infrared detectors below.

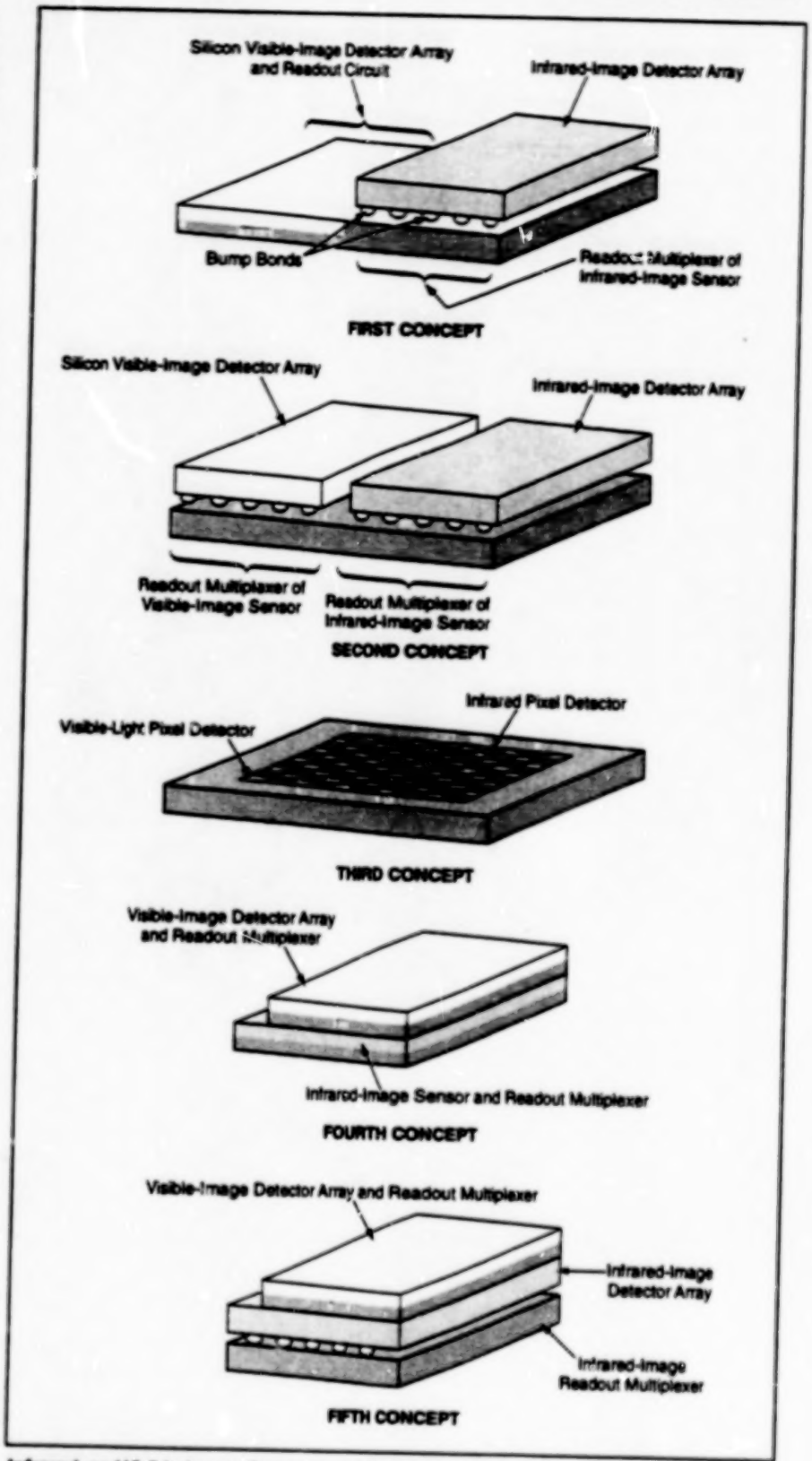

Infrared- and Visible-Image Sensors would be integrated. Pixel detectors could be arranged in side-by-side subimages or else interspersed or superimposed in the same image area.

Registration of the infrared and visible pixel detectors could be achieved readily; however, whether or not they were registered, it would not be necessary to make them with equal pixel pitches. Wire bonds could be made between the two sensor chips to enable sharing of signals or sensor-fusion data processing on one or both chips. The fifth concept is similar to the fourth concept, except that the infrared sensor would be implemented in a hybrid structure.

This work was done by Eric Fossum and Bedabrata Pain of Caltech for **NASA's Jet Propulsion Laboratory**. *No further documentation is available.*
NPO-20219

Inflatable Reflectarray Antennas

Reflector surfaces are stretched flat by inflating circular toroidal tubes.

NASA's Jet Propulsion Laboratory, Pasadena, California

Inflatable Circular Toroidal Tubes stretch the planar array of microstrip patches printed on a circular membrane.

A type of reflectarray antenna now undergoing development is based on the concept of a reflector membrane that is stretched flat by attaching it to an inflatable frame (see figure). Antennas of this type are meant to serve as lightweight, compactly stowable, reliable alternatives to conventional antennas with rigid reflector structures or mechanically deployed mesh reflectors. Originally intended for use aboard spacecraft for microwave communications, these antennas might also prove useful in terrestrial low-power, lightweight microwave systems in cases in which reflector-surface distortions caused by gravitation and wind could be tolerated.

The reflectarray in an antenna of this type is a planar array of microstrip patches printed on a thin circular membrane. An inflatable circular toroidal tube is attached to the edge of the membrane; when inflated, the tube stretches the membrane flat and supports the membrane in the operational configuration. Inflatable tripod tubes attached to the inflatable torus serve as struts to support a feed horn that illuminates the reflectarray. The patches of the reflectarray are shaped and sized to make the reflected electromagnetic field cophasal, so that the antenna operates with high gain.

It must be emphasized that surface of an antenna of this type is designed to be flat — in contradistinction to the paraboloidal shape of a conventional antenna reflector. In a previous attempt to deploy an inflatable antenna with a paraboloidal reflector surface, the surface figure deviated from the required paraboloid by far more than the maximum allowable error. In the present case, achievement of the desired precision in the surface figure is not difficult; the desired flatness is readily maintained by stretching the membrane.

A prototype with an overall size of about 1 m, designed for operation in the X band, has been built and tested. The inflatable antenna structure should be mass-producible at low cost.

This work was done by John Huang and Alfonso Feria of Caltech for **NASA's Jet Propulsion Laboratory**. *Further information is contained in a TSP [see page 1].*
NPO-20433

Filtering To Increase Effective Yields of Image Sensors

Median filtering in small neighborhoods would reduce effects of the most common faults.

NASA's Jet Propulsion Laboratory, Pasadena, California

The addition of special-purpose signal-processing circuitry has been proposed to overcome some of the deleterious effects of hardware faults in integrated-circuit image sensors of active-pixel-sensor (APS) type and possibly of other types. The mathematical basis of the method is median filtering in a small neighborhood (typically of 3 × 3 or 5 × 5 pixels) centered,

in turn, on each pixel; that is, one seeks to replace the intensity signal for each pixel with the median-intensity signal for its neighborhood. From the perspective of a human observer viewing the image on a remote video display, such median filtering would reduce or eliminate the visible effects of malfunctioning single pixels or of malfunctioning rows or columns of single-pixel width — the faults most commonly observed in large state-of-the-art integrated-circuit image sensors. Thus, the effective production yields of the image sensors would be enhanced.

Heretofore, neighborhood median filtering has usually been implemented by software in the first stage of processing of digitized pixel signals. In the proposed method, the median filtering would be implemented in hardware; more specifically, by use of additional electronic circuitry that would be installed on the periphery of the image-sensor area. In comparison with the software implementation, the proposed hardware implementation would offer the advantage of reduced computational burden and possibly greater processing speed.

The figure shows a simplified layout for implementing median filtering in 3 × 3 neighborhoods. The intensity signals from pixels would be read out row by row and initially stored in a three-row buffer. Each cycle of operation would begin with reading signals from a new row into the buffer, accompanied by dropping the signals from the oldest row from the buffer. Units containing analog circuits with timed, transistor-switched, access to adjacent 3 × 3 neighborhoods in the buffer would then identify and pass on the median intensity signals from these neighborhoods. These units would operate on each group of three rows in three phases as follows:

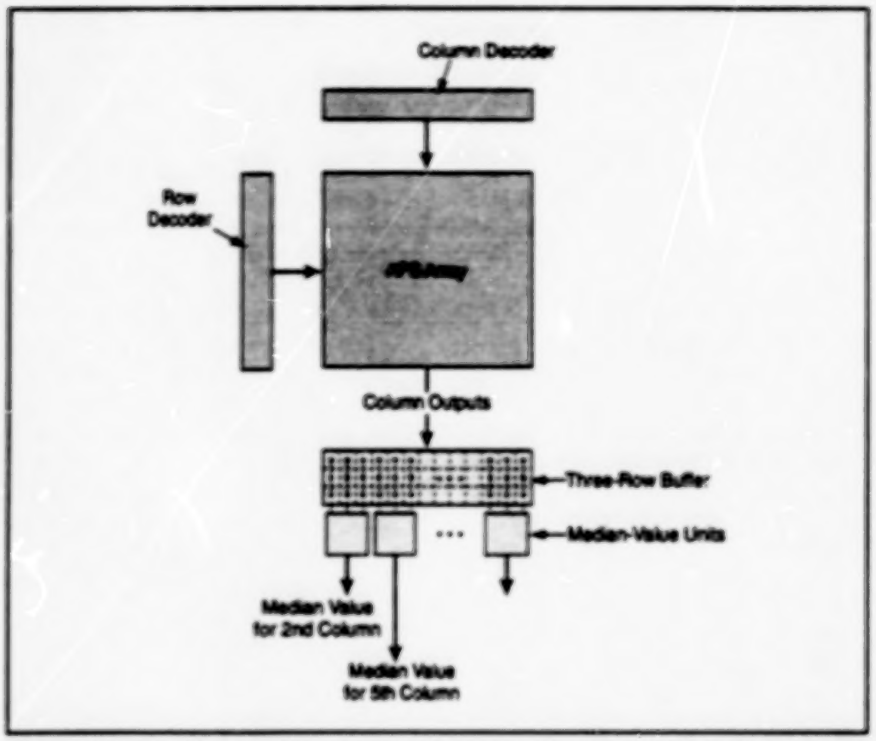

Median-Intensity Values would be stored in a three-row buffer, then found for pixels in adjacent 3 × 3 neighborhoods along the middle row in the buffer. A three-phase cycle, with incrementing of the column locations by one step in each phase, would be necessary to obtain all the median values for the row in question.

During the first phase, the units would put out the median values associated with the middle row in the buffer and with the columns in the numerical sequence 2, 5, 8, and so forth. In the third phase, columns in question would be those in the numerical order 3, 6, 9, and so forth. In the third phase, the columns in question would be those in the numerical order 4, 7, 10, and so forth. Upon completion of the third phase, all available median values for the middle row in the buffer would have been generated. Then a new cycle would begin with loading of a new row into the buffer and with the row loaded on the previous cycle becoming the new middle row.

This work was done by Orly Yadid-Pecht, Bermuk Mansoorian, and Bedabrata Pain of Caltech for **NASA's Jet Propulsion Laboratory**. *Further information is contained in a TSP [see page 1].*
NPO-20211

Frequency-Scanning Capaciflectors

Capacitive proximity sensors could be used to identify materials.

Goddard Space Flight Center, Greenbelt, Maryland

Capacitive proximity sensors of this proposed type would be based on the capaciflector concept, with an extension of hardware and software designs to incorporate capabilities for scanning in frequency and analyzing the resulting capacitance-vs.-frequency data. The proposed frequency-scanning sensors would perform all the functions and offer all of the advantages of capaciflectors; in addition, they would provide information on materials within their capacitive-sensing ranges.

Capaciflectors and related topics have been described in a number of prior arti-

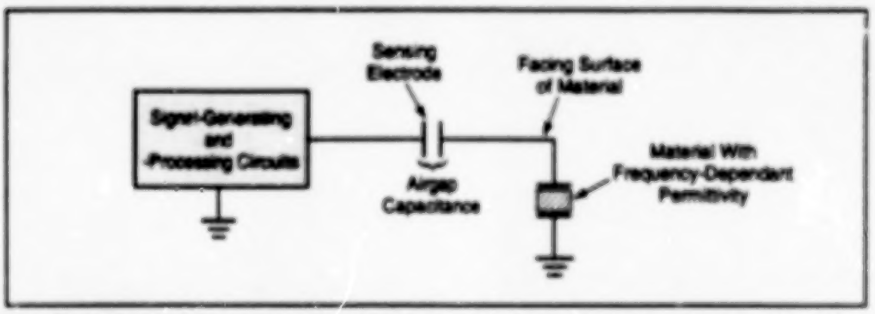

The **Capacitance Measured** via the sensing electrode can be approximated as a series combination of two capacitances, one of which is proportional to the frequency-dependent permittivity of the material of the sensed object. The material can thus be identified from the frequency dependence of the measured capacitance.

cles in *NASA Tech Briefs* during the past several years. A typical capacifector includes a sensing electrode and a driven shielding electrode, both excited at the same voltage, frequency, and phase via voltage followers. The voltage follower that drives the sensing electrode also includes an operational-amplifier circuit for measuring the sensing-electrode current, which includes a component proportional to the excitation voltage and to the capacitance between the sensing electrode and any objects in the vicinity.

The figure illustrates the basic measurement principle of a frequency-scanning capacifector. In the case of a nearby dielectric object, the sensed capacitance can be regarded as two capacitances in series: an airgap capacitance between the sensing electrode and the facing surface of the object, and a capacitance between the facing surface of the object and electrical ground. The dc values of these capacitances depend partly on the geometry of the electrode and the object. The ac capacitance through the object is proportional to its dc capacitance and varies with frequency according to the frequency dependence of the permittivity of the object material. Thus, it is possible to use the shape of the measured capacitance-vs.-frequency curve to differentiate between the effect of geometry and the effect of the object material, and to distinguish among materials with different permittivity-vs.-frequency curves.

A computer could store data on capacifector responses as functions of frequency for sensed objects made of a variety of known materials. Then the computer could compare data from a capacifector frequency scan with the stored data by use of a mean-square estimator with the amplitude of the frequency response as a free variable:

$$\min_{a,m}\Sigma(ar_{f,m} - c_f)^2,$$

where a is the unknown amplitude, $r_{f,m}$ is the stored frequency response of the mth material at frequency f, and c_f is the measured capacifector response (sensing-electrode current or proportional signal) at frequency f. That is, the computer could choose a combination of amplitude and material to minimize the mean squared error between the measured response c_f and the stored response $r_{f,m}$.

Some applications for this sensor include rapid determination of rock types, determining the type of snow and ice accumulation on aircraft wings, and determining if passengers are carrying weapons or explosives.

This work was done by Charles E. Campbell, Jr., of **Goddard Space Flight Center**. *Further information is contained in a TSP [see page 1].*

This invention is owned by NASA, and a patent application has been filed. Inquiries concerning nonexclusive or exclusive license for its commercial development should be addressed to the Patent Counsel, Goddard Space Flight Center [see page 1]. Refer to GSC-13618.

Hybrid Imaging Technology

Devices are made from CCD and CMOS components, which can be independently optimized.

NASA's Jet Propulsion Laboratory, Pasadena, California

"Hybrid imaging technology" (HIT) is the name of a discipline in which the advancement of electronic image sensors is pursued via hybridization of charge-coupled-device (CCD) and complementary metal oxide/semiconductor (CMOS) circuitry. The guiding principle of HIT is to combine CCD and CMOS components into units that afford capabilities that neither CCD nor CMOS circuitry can provide by itself. HIT can be applied to advantage in almost any situation in which there are requirements for very high imaging quality and low power dissipation. Applications can include portable video and portable digital still cameras, remote surveillance cameras, and low-power cameras in spaceborne and terrestrial scientific instrumentation.

HIT merges the exceptional quantum efficiencies, fill factors, broad spectral responses, and very low noise levels of CCDs with the low power levels, system-integration capabilities, and low costs of CMOS-based active-pixel sensor (APS) circuits to create the next generation of high-performance image sensors. Some of the related research outside HIT has included attempts to merge CCD and CMOS components at the device-fabrication-process level. Although these attempts have yielded working image sensors, the devices have exhibited poor image quality and high noise because of lack of optimization of CMOS processes. In turn, the lack of optimization has been due to a basic incompatibility between CCD and CMOS processes as they relate to processing temperatures and to required oxide thicknesses for CMOS transistors.

An essential element of the HIT approach is that no attempt is made to unite CCD and CMOS devices at the device-fabrication-process level; instead, the CCD and CMOS components of a given device are fabricated in separate CCD and CMOS processes and then joined mechanically and electrically (hybridized) by bump bonding. This element of HIT makes it possible to avoid costly process development. This approach also makes it possible to optimize the CCD and the CMOS parts independently, in such a way as to maximize the overall performance of the resulting image sensor in a highly miniaturized format.

Another advantage of HIT is that it enables the reuse of CCD imaging devices and CMOS readout circuitry without need for costly refabrication. A supply of unhybridized components can be maintained so that combinations of components can be selected to satisfy requirements in specific applications.

The imager integrated-circuit chip of an HIT image sensor is essentially a CCD chip, except that the on-chip amplifier usually found in such a device has been replaced by either a floating diffusion or a floating gate output node. The companion CMOS chip must contain a charge-to-voltage conversion amplifier similar to an operational amplifier configured as a charge integrator. Depending on the application, the CMOS chip could also contain additional circuitry to perform such functions as correlated double sampling and analog-to-digital conversion. Matching bump-bond pads are formed on the CCD imager and CMOS chips during their respective fabrication processes. Indium bumps are deposited on the pads, and the chips are joined by standard bump-bonding techniques.

This work was done by Mark V. Wadsworth of Caltech for **NASA's Jet Propulsion Laboratory**. *Further information is contained in a TSP [see page 1].*
NPO-20542

High-Speed Image Detectors With Subelectron Noise Floors

Hybrid devices exploit the best of CCDs and CMOS circuits.

NASA's Jet Propulsion Laboratory, Pasadena, California

Parallel ultra-low-noise hybrid detectors (PHUDs) are developmental image-detector devices for use in low-power, scientific-grade video cameras. The hybrid nature of a PHUD lies in the incorporation of both charge-coupled-device (CCD) image-detection circuitry and complementary metal oxide/semiconductor (CMOS) parallel readout circuitry. PHUDs promise to revolutionize optical spectrometers and related instruments by providing low-noise, single-photon detection capabilities at conveniently high video data rates.

Until now, subelectron-noise, single-photon-detection capabilities have been achieved by multisampling, nondestructive readout from CCDs. The major disadvantage of this approach is slowness, because of a need to sample each data packet 10 to 100 times in serial fashion; readout rates have been of the order of 5×10^4 pixels per second, resulting in readout times of tens of seconds per frame for typical images of 800 × 800 pixels. In principle, multisampling could be speeded by performing it in parallel instead of serial fashion, but attempts to implement parallel sampling have resulted in excessive power consumption (>1 W per CCD) and consequent excessive heating that degrades device performance.

In contrast, PHUDs are designed to achieve low noise (<1 electron root mean square), and readout rates of the order of 10^6 pixels per second while consuming less than 50 mW per device. The key design concept of PHUDs is exploitation of the best features of both CCDs and of CMOS imaging devices:

- CCD Features — High quantum efficiency, broad spectral response, low readout noise, high resolution, and large format.
- CMOS Features — Low power consumption, capability for on-chip implementation of such additional functions as digitization and multiplexing, and compatibility with external CMOS circuitry.

The design of a PHUD involves not only hybridization of CCD and CMOS components but also departures from conventional designs of these components. The conventional high-speed serial register is removed from the CCD, a charge-conversion structure is incorporated at the output end of each column in the CCD, and a high-speed CMOS multiplexer for output of voltage-domain signals is added. The signal charge is sensed by a floating polysilicon gate or other suitable nondestructive sensing node located within the CCD at the output end of each column. Charge conversion occurs simultaneously for all columns of pixels. The charge packet in each pixel in a given row and column is measured N>1 times on the sensing node of the column, and each measurement is stored in the CMOS chip by means of an averaging circuit; the resulting readout noise is approximately $N^{-1/2}$ times what it would otherwise be. Because this multiple sampling occurs simultaneously for all pixels along a row, the overall frame rate is not appreciably diminished.

Column-to-column variations in signal offsets and gains in a PHUD can readily be corrected in the course of routine digital processing of readouts. Calibration data for use in computing the corrections are averages and variances of readouts from uniform images.

This work was done by Mark V. Wadsworth of Caltech for **NASA's Jet Propulsion Laboratory**. *Further information is contained in a TSP [see page 1].*
NPO-20576

Improved Control of Charging Current for Ni/H Battery

Charging current would be tapered off at the onset of overcharge to limit heating.

NASA's Jet Propulsion Laboratory, Pasadena, California

In a proposed method of controlling the electric current supplied for charging a nickel/hydrogen battery, the rate of evolution of heat would be taken into account along with the electrical quantities (voltage, current, and/or charge as functions of time) that are traditionally taken into account. This method might also prove useful for controlling charging currents in batteries based on different chemistries.

The parameters related to limitations on the lifetime of an Ni/H battery are depth of discharge, temperature, and overcharge. The major proximate cause of failure is gradual swelling of plates, associated with overcharge and with the generation of oxygen in the overcharge reaction sustained over thousands of charge/discharge cycles. In principle, the lifetime could be prolonged by minimizing overheating and precisely limiting the amount of overcharge.

The rate of heating cannot be measured directly but can be estimated from other quantities that can be measured. Because an Ni/H cell is a pressure vessel, its internal pressure can be used as an indication of the amount of hydrogen present and thus of the state of charge. Assuming that (1) the void volume in the battery remains constant; (2) the pressure, temperature, and number of moles of hydrogen are related by the ideal gas law; and (3) the charging efficiency is 100 percent, then the rate of increase of pressure during charging should be proportional to the rate of charging; that is, to the charging current.

Any deviation from this proportionality would be attributed to a decrease in efficiency associated with the overcharge reactions. The portion of applied current diverted to the overcharge reaction would not be available for the main charging reaction that generates hydrogen; as a consequence, for a given charging current and temperature, the rate of increase of pressure would decrease as the battery went into overcharge. The oxygen generated in part of the overcharge reaction is also quickly recombined in another part of the overcharge reaction; the net effect of the portion of the charging current diverted to the overcharge reaction is to generate heat. Thus, by use of basic equations of thermodynamics, it should be possible to determine the charging efficiency and the rate of generation of heat from measured values of pressure, temperature, and voltage as functions of time.

The proposed method would be imple-

mented in control software. In this method, the rate of generation of heat computed as described above would be used as feedback in a control algorithm that would taper the charging current to maintain the lowest possible battery temperature and minimize the generation of oxygen. The maximum allowable rate of generation of heat would have to depend on the temperature of the battery because charging efficiency decreases with increasing temperature.

This work was done by Paul Timmerman of Caltech for **NASA's Jet Propulsion Laboratory.** *Further information is contained in a TSP [see page 1].*

NPO-20470

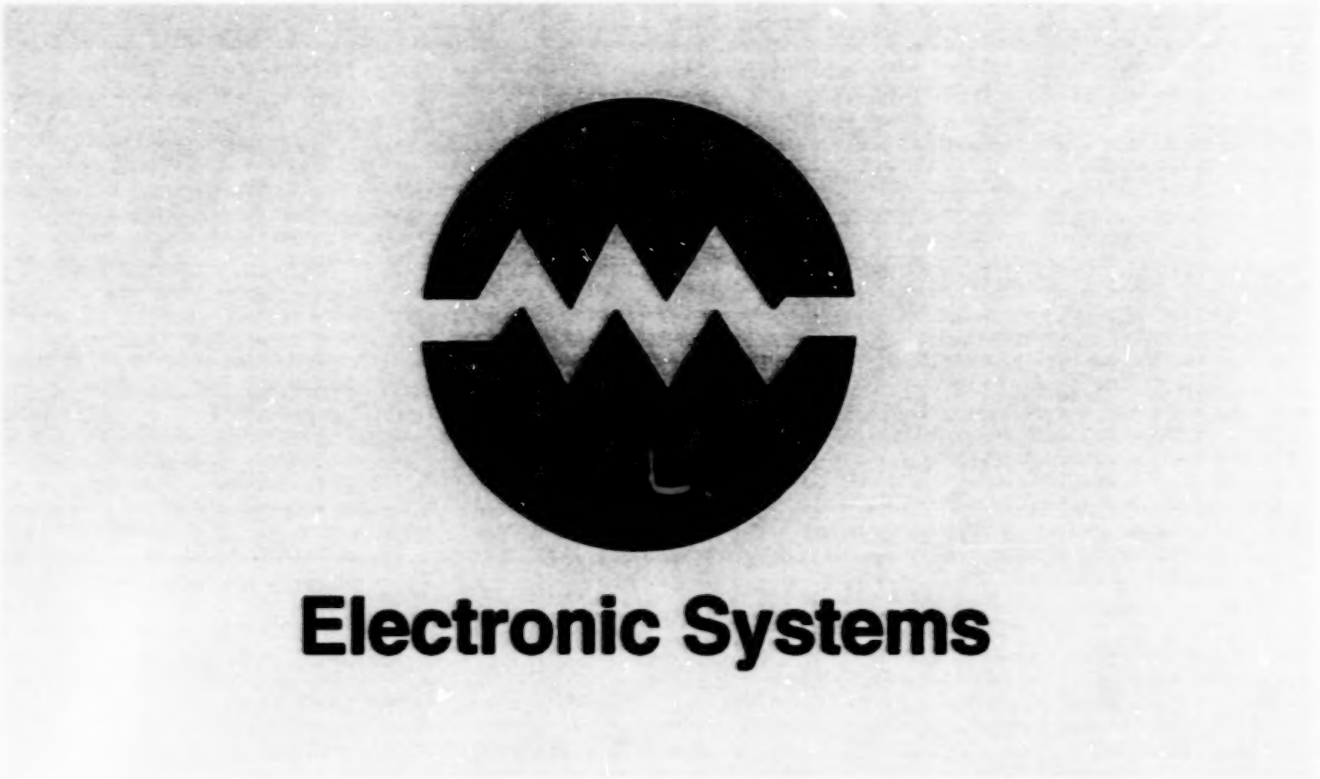

Electronic Systems

Hardware, Techniques, and Processes

17 Low-Power, Moderate-Speed Serial Data Communication Link
18 Sensor Webs
19 Fast Transient-Voltage Recorder
20 Fault-Tolerant Feedback System for Robot Control
21 Third-Generation Data-Acquisition System Now in Operation
22 Data-Acquisition System Takes 8-Bit Samples at 1 GHz

Books and Reports

23 Evolvable Multiagent Approach to Spacecraft Communication

BLANK PAGE

Low-Power, Moderate-Speed Serial Data Communication Link

Characteristics include low mass, low volume, low noise, and low power consumption.

Goddard Space Flight Center, Greenbelt, Maryland

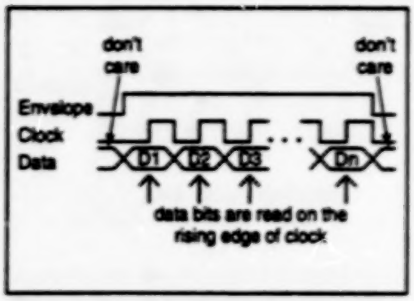

Figure 1. The Data-Shifting Scheme incorporates differential signals that include clock, data, and envelope signals.

A low-power serial data communication link has been designed to transmit data among subsystems of a spacecraft instrumentation system, at rates up to 5×10^5 bits per second. The design of the link is adaptable to other spacecraft systems and to terrestrial applications that include cellular telephones, laptop computers, and other compact, lightweight digital electronic consumer products.

The design had to satisfy requirements for low power consumption, small volume, small mass, and radiation hardness. Signals were required to be transmitted via differential networks to help minimize noise effects. The link was required to function over data-transmission lengths up to 1 m, and in the presence of potential differences of as much as 0.5 V between receiver and transmitter electrical grounds. In addition, there was a requirement that subsystems on the network that were powered down could not become powered up through the serial link.

The differential signals in the link include a clock signal, a data signal, and envelope signals (see Figure 1). An envelope signal becomes active at one-half period before the first rising edge of the clock signal and remains active until the end of the ensuing transfer of data. Data bits are valid on the rising edges of the clock signal.

The serial link includes a master subsystem that transmits commands to, and receives telemetric data from, numerous slave subsystems. Because there is a single source of commands and there are multiple sources of telemetric data, the serial link is divided into a command portion that includes a transmitting differential network [see Figure 2(a)] and a telemetry portion that includes a receiving differential network [see Figure 2(b)]. For each portion, there are two design options: one for data rates up to 2×10^4 bits per second,

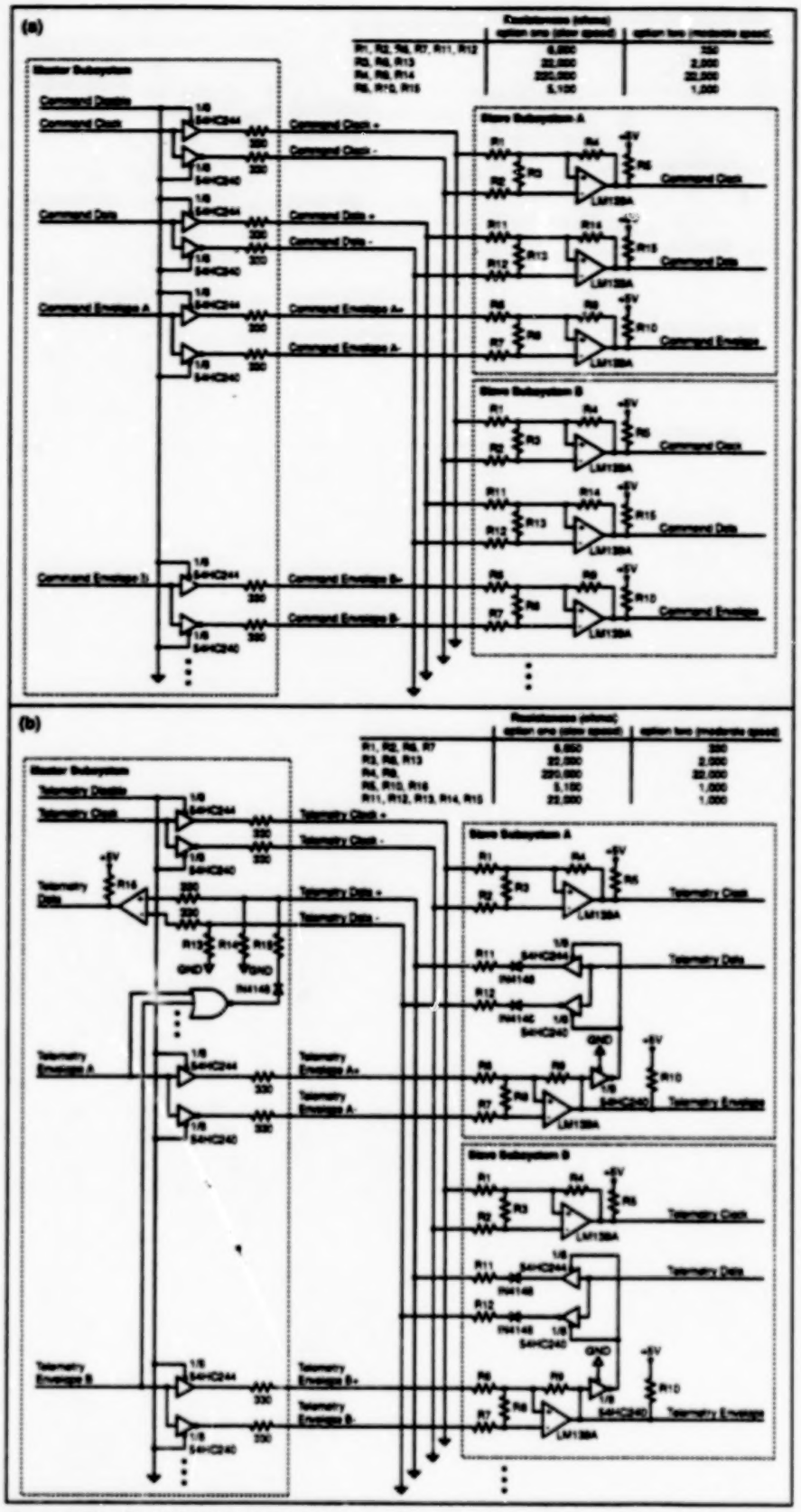

Figure 2 The Serial Link includes (a) transmitting differential network and (b) receiving differential network.

and one for data rates up to 5×10^5 bits per second. The higher-data-rate option involves smaller resistance values and thus higher power consumption. In both portions, all slave subsystems receive the same clock and data signal pairs, while each slave subsystem receives its own envelope signal pair. Each envelope signal pair indicates the subsystem to which the data are to be sent.

The serial link offers the following advantageous features in addition to those mentioned above:

- The circuitry includes LM139A comparators with feedback resistors connected to them to add hysteresis and thereby provide some immunity to noise. This feature is useful if the differential inputs to a comparator are differentially delayed because of differences in lengths of signal conductors.
- Voltage dividers connected to the comparator input terminals allow slave subsystems' ground potential to differ from the master subsystem's by as much as 1 V.
- All current loops carry small currents. The comparator input currents are smaller than 1 μA. The current flowing between any two subsystems is smaller than 5 mA. Interference and grounding problems associated with current loops are therefore less severe than they might otherwise be.
- Options are available by varying the basic design. Command and telemetry clock signals can be combined into a single clock-signal pair to reduce complexity. Similarly, the command and telemetry envelope signals for a subsystem can be combined into a singe signal pair. These changes lead to simultaneous transmission and reception. Other options include the use of part of the slave circuit design in the master in the event that only one source of telemetry data is used, modifications to enable the slave to be unpowered while the master is powered, and an alternative design that calls for LM119A comparators to increase the speed of the network beyond that achievable with LM139A comparators.

This work was done by Kenneth W. Wagner of **Goddard Space Flight Center**. *Further information is contained in a TSP [see page 1].*
GSC-13926

Sensor Webs

Notable features would include flexibility of deployment, low power consumption, and low cost.

NASA's Jet Propulsion Laboratory, Pasadena, California

Sensor webs are developmental collections of sensor pods that could be scattered over land or water areas or other regions of interest to gather data on spatial and temporal patterns of relatively slowly changing physical, chemical, or biological phenomena in those regions. Each sensor pod would be a node in a data-gathering/data-communication network that would span a region of interest. Each sensor pod would contain two modules: (1) a transducer module that would interact with the environment to gather the desired data and (2) a communication module.

The basic concept of a network of sensors is not new. The novelty of the sensor-web concept lies in exploitation of a confluence of advances in integrated circuits for radio communication, wireless-network communication technology, and cheap micromachined sensors. This exploitation takes the form of a design concept that affords flexibility of configuration and operation of networks while minimizing power consumption.

A sensor web would contain a few primary nodes and many secondary nodes. Data would be transferred from node to node within the network. The primary nodes would have the additional capability and task of communicating signals into and out of the sensor web: For example, at a primary node, sensory data gathered by the web could be transmitted to an overhead aircraft or satellite or to a local field computer.

Inasmuch as the power needed for intraweb transfer of data increases with the bandwidth of the sensor signals, the sensor output signals should be of low bandwidth to make it possible to minimize power consumption in the sensor pods. Fortunately, many natural phenomena that one might wish to monitor (e.g., temperature or concentrations of chemicals) are inherently of low bandwidth. In cases of phenomena that vary more rapidly, it could be necessary to compress the sensor data at the nodes before transmission.

The use of intraweb, node-to-node communication would reduce the power needed to transmit data out of a web. It would also make it possible to reduce the energy consumed by power-hungry sensors: Web nodes could query each other to track the movements of microclimatic or other fronts over the web, so that power-hungry sensors could be activated only when a front is known to be passing. In other words, intraweb communication enables a nonlinear increase in the value of the local data collected in much the same way that an aggregate of neurons exhibits more intelligence than does a single neuron. Moreover, the synergistic interaction among many separate node transducers would increase the value of the collected data by providing instantaneous correlation across the web.

A sensor web would not be inherently restricted to contain a specific number of nodes or to operate within predefined area. The primary nodes could be located anywhere in the network, and multiple webs deployed in a given area would naturally mesh with one another. A sensor web could be regarded as instrument, the surveying area of which could be expanded by multiple deployments of nodes.

A sensor web would be a relatively cheap instrument because sensor pods could be mass-produced, taking advantage of economies of scale. Because of this cheapness, individual sensor pods could be regarded as expendable. As a further consequence, it would be possible to "reseed" a sensor web with fresh nodes to replace ones that have failed; thus, the sensor web could be repeatedly renewed, enabling it to operate for an indefinitely long time.

A sensor web could be made as redundant and/or as dense as desired by simply distributing as many nodes as desired over a given survey area. Redundancy would, of course, render the sensor web tolerant to failures of individual pods. High density could be utilized to achieve high spatial resolution and/or to obtain statistically significant numbers of data when surveying biological or other phenomena that are inherently stochastic.

Sensor webs could be useful in almost any endeavor in which there is a need for low-power, low-bandwidth, long-term monitoring over large areas. For example, they could be used to monitor microclimates and concentrations of nutrients for agricultural purposes, to track flows of toxins in ground water, to monitor traffic, or to monitor seismicity in a survey area.

This work was done by Kevin Delin, Shannon Jackson, and Raphael Some of Caltech for **NASA's Jet Propulsion Laboratory**. *Further information is contained in a TSP [see page 1].*
NPO-20616

Fast Transient-Voltage Recorder

This instrument responds rapidly enough to record transients induced by lightning.

John F. Kennedy Space Center, Florida

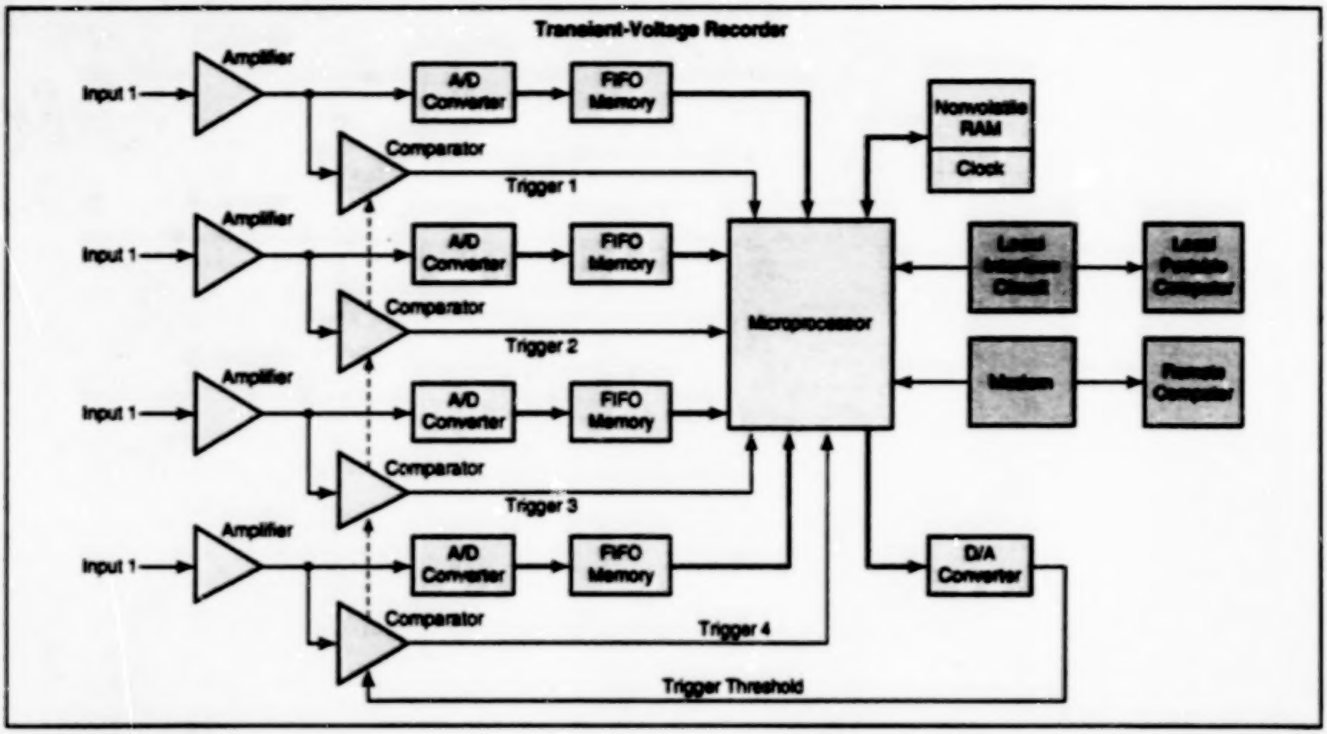

This **Transient-Voltage Recorder** offers rapid-sampling, pretrigger recording, and rapid-rearming capabilities needed for accurate recording of lightning-induced transients.

The figure schematically illustrates an instrument designed expressly for recording lightning-induced transient voltages on power and signal cables. The principal advantage of this instrument over previously available transient-voltage recorders is high speed, as explained below.

Transient voltages generated by large electric motors and switching of power equipment consist primarily of spectral components well below a frequency of 1 MHz. Most commercial transient-voltage recorders can detect and record such transients. However, transients induced by lightning feature voltage peaks with rise times of fractions of a microsecond; in other words, they contain significant spectral components above 1 MHz. Commercial transient-voltage recorders do not respond rapidly enough to measure and record lightning-induced transients accurately.

The present transient-voltage recorder samples transient voltages in four channels at a rate of 20 MHz. The instrument can handle a peak input potential of 50 V, or more if an attenuator is used.

A microprocessor controls the operation of the instrument. A trigger circuit continuously monitors the signals on all four channels, comparing the signal level on each channel with a predetermined threshold level. The threshold for each channel can be set at any level from 5 to 95 percent of full scale, independently of the threshold levels for the other channels. When the signal level in any channel exceeds its threshold level, a trigger signal is generated, causing full recording of data to begin simultaneously on all four channels.

Even when data are not being recorded fully, the analog-to-digital (A/D) converters in the four channels operate continuously, temporarily storing their output data in first-in/first-out (FIFO) memory circuits that are always kept half full. When a trigger signal is received, the remaining halves of the FIFO memories are filled up with data. Inasmuch as the full capacity of each FIFO memory corresponds to an observation interval of 200 μs, this arrangement provides a 100-μs pretrigger recording capability. Once a transient has been thus recorded, the data are transferred to a nonvolatile random-access memory (RAM). The instrument is then rearmed for triggering within 400 μs to record subsequent transients; such a rapid-rearming capability is necessary because a lightning strike can generate multiple transients at intervals of a few milliseconds.

The instrument is equipped with a clock, and the stored data are time-coded, not only to establish the times of transients but also to facilitate correlation with data on the same transients measured by other instruments. Data on as many as 15 transients can be stored in the RAM. The data are retrieved from the nonvolatile RAM, either locally by use of a portable computer and a standard interface circuit, or remotely through a modem. The instrument is normally powered through an ordinary ac power line but also contains batteries to enable it to operate as long as 16 hours in case of ac-power failure. The nonvolatile RAM retains its data even when the batteries have been depleted.

This work was done by Howard James Simpson and Pedro J. Medelius formerly of I-NET, Inc., for **Kennedy Space Center.** *No further documentation is available.*

Inquiries concerning rights for the commercial use of this invention should be addressed to the Technology Programs and Commercialization Office, Kennedy Space Center, (407) 867-6373. Refer to KSC-11991.

Fault-Tolerant Feedback System for Robot Control

This system takes corrective action when transducers are found to be defective.

Lyndon B. Johnson Space Center, Houston, Texas

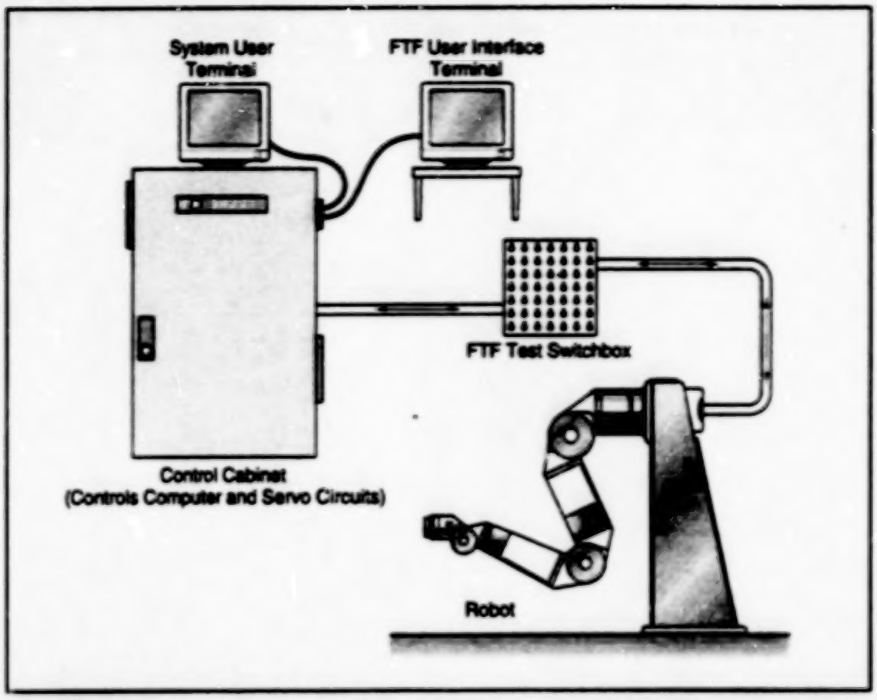

The FTF System is an integral part of the robot-control system. It detects erroneous transducer signals and modifies the control laws accordingly to help ensure safe operation and increase reliability.

A fault-tolerant feedback (FTF) system has been integrated into a robot control system to prevent robot-arm runaways that could be caused by failure of one or more transducers such as joint-position, torque, and motor-temperature sensors, or in associated wiring harness channels. The FTF system responds to a transducer failure by commanding either safety shutdown or else continued operation of the robot in a degraded mode. The FTF system can detect errors in joint-position, velocity, and torque feedback signals far more quickly than older systems can, thereby reducing uncontrolled motion of the robot arm before a shutdown command is executed. The FTF system can help to ensure safe and efficient operation of a robot that must share its workspace with humans and with delicate materials and equipment.

The FTF system is implemented on a single processor circuit board that plugs into the backplane of the robot-control computer and that operates between the motion-controller and servo-processor subsystems of the robot-control system. An analog-to-digital input circuit board and analog buffer/filter circuit board are also used to acquire data. All additional data and control capability required by the FTF system are available through a servo-level interface circuit. The FTF system also includes a user interface that comprises a video display terminal and a keyboard (see figure).

The FTF intercepts robot-joint-position commands from the motion controller to the servo processor. It also evaluates feedback information from the servo processor and the input board every 10 milliseconds. By use of a mathematical model of the servo system, the feedback signals are compared to each other to determine whether any transducers have failed.

The comparison of transducer signals occurs after the signals have been processed through second-order Butterworth filters. The filter frequency is selected so that only information below the natural frequency of vibration of the robot-drive mechanism is evaluated. This is essential when motor and axis information is compared and helps to eliminate false error indications caused by noise, nonlinearities, and dynamical error in the mathematical model. The differences between the actual signals and the signals computed from the model are compared to predetermined tolerances specified by the operator. When one of these differences exceeds the applicable tolerance, an error (and thus a transducer failure) is deemed to have occurred, and the FTF responds accordingly.

When no transducer failure has been detected, the FTF passes the commands unchanged to the servo processor. When a transducer failure has been detected as described above, then depending on the current mode of operation, the FTF system either immediately disables the robot or else executes a different control law for the affected coordinate axis, eliminating the use of the faulty transducer. The execution of the different control law is accomplished by use of feedback information from the servo processor, information from the mathematical model of the servo system, and the position command from the motion controller. The FTF system then sends a motor-current command instead of a joint-position command for the affected axis to the servo processor. With respect to the remaining axes, for which transducer failures have not been detected, the control system continues to operate normally.

The FTF system can be made to operate in any of three modes called "safe," "battlefield", and "disabled." In the safe mode, the FTF system immediately disables the robot upon detection of any error. This mode is used when it is crucial that the manipulator not collide with objects in the workspace and provides a great increase in safety over other robotic systems. The battlefield mode provides for continued operation, with some degradation of performance, after a transducer failure. This mode significantly increases the reliability of the robotic system but at the expense of performance and safety. The disabled mode is used for calibration of the FTF system and evaluation of the performance of the rest of the robotic system (that is, with the FTF system excluded).

This work was done by Paul H. Eismann, James P. Karlen, and Talt Blevins of Robotics Research Corp. for **Johnson Space Center**. *Further information is contained in a TSP [see page 1].*
MSC-22591

Third-Generation Data-Acquisition System Now in Operation

Setup of test data bases, recording of data, display functions, and troubleshooting are simplified.

Dryden Flight Research Center, Edwards, California

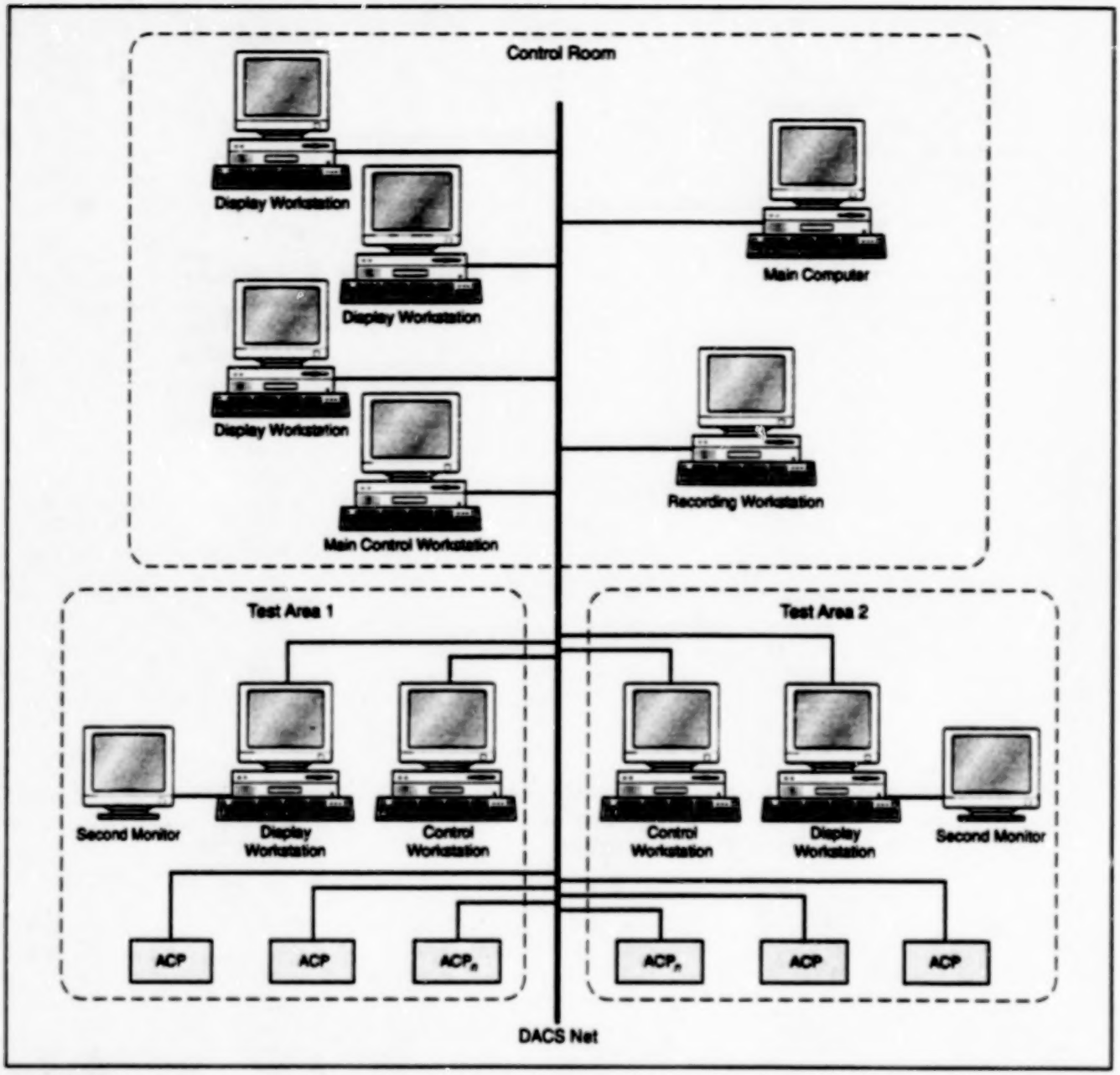

The DACS III is essentially a network of computers, computer workstations, and data-acquisition circuits. This system contains standard components that can be easily replaced with newer versions.

Dryden Flight Research Center's Flight Loads Laboratory (FLL) was constructed in 1964 for use in performing combined mechanical and thermal tests of structural components and complete flight vehicles. The FLL is also used to calibrate and evaluate flight-loads instrumentation under the conditions expected in flight. The required testing is performed by the FLL's data-acquisition and control system (DACS).

A major portion of the FLL's third-generation data-acquisition and control system (DACS III) has been placed in service. This system is being developed in phases through the combined effort of a team composed of both civil-service and contractor personnel. The second-phase version of the system — now fully operational — performs data-acquisition, display, and replay functions, and provides troubleshooting tools. The DACS III provides enhanced capabilities that greatly increase productivity and efficiency.

The DACS III (see figure) consists mostly of a network of computers and workstations linked in a manner to pro-

vide maximum flexibility. This system has been designed to prevent obsolescence by use of industry-standard components that can be easily replaced when newer versions are introduced. An extensive use of graphical-user-interface (GUI) techniques simplifies test-setup definitions (test scenarios) as well as test operations and troubleshooting. A minimum time of two to three days was needed to generate a scenario for a typical test by use of the previous DACS. Operators can now generate the same test scenario in two to three hours by use of the DACS III.

The DACS III includes at least one acquisition-and-control processor (ACP) based on the VersaModule Eurocard (VME) and uses WindRiver's Vxworks real-time operating system. An installed Inter Range Instrumentation Group B (IRIG-B) interface card provides time stamping of sampled data. The data-acquisition system can be scaled up to 1,280 channels by using multiple ACPs, and operates at rates that vary from 10 to 160 samples per second.

This system has been designed to function in an environment that includes harsh electrical noise. All analog inputs are fed to the ACP(s) through fiber-optic cables to reduce electromagnetic interference. Each analog input module is an independent analog-to-digital (A/D) converter that generates 16-bit data by the sigma-delta conversion method. All A/D modules feature 1,500-volt isolation and 100 dB of normal-mode rejection at a frequency of 60 Hz.

Each ACP provides local recording of raw data and real-time conversion of engineering units. A key feature of the system is its ability to broadcast engineering-unit-converted data over an Ethernet. These data can be displayed throughout the laboratory on workstations that are equipped with the appropriate display software and attached to the DACS network.

The DACS III includes a data-display system that provides distributed real-time data displays updated at a rate of 5 samples per second. A user can choose several displays that can be overlaid on the same screen. All display parameter entries are driven by a GUI. The following types of displays are available: alphanumeric, x-y plots, vector, bar graph, force-stiffness, and derived parameter. All display engineering workstations are equipped with 21-in. (53-cm) monitors.

Control engineering workstations provide centralized control of test and recording processes for associated ACPs. Calibration functions, troubleshooting, event displays and record control are all available at these stations. The main control workstation performs the same functions as do the control engineering workstations, and offers the additional capability to control any or all of the ACPs.

A recording workstation is dedicated to recording the broadcast data from the ACPs. The recorded information is saved in a format that makes it available, immediately following a test, for evaluation by use of plotting software developed at Dryden Flight Research Center.

The DACS III includes a main computer (not to be confused with the main control computer) that is used for processing raw or engineering-unit-converted data logged during a test run. This computer also serves as the engine for all data-base functions.

One final feature worthy of note is a test-replay option, which enables research engineers to replay portions or all of a test run following a test. The replay can be at the original broadcast speed or slower. Full data-display functions are available during replay. There is also an option to generate displays during replay that were not used during the original test run; this option makes it possible to examine data of interest at a greater level of detail than what was available during the test run.

This work was done by Alphonzo J. Stewart, Allen Parker, Jr., Knut Roepel, and Van Tran of **Dryden Flight Research Center** *and Manuel Castro, Ronald Rough, and Chris Talley of the Woodside Summit Group. For further information, write to Alphonzo J. Stewart, NASA Dryden Flight Research Center, P. O. Box 273, Edwards CA 93523; call (805)258-3579; or send electronic mail to al.stewart@dfrc.nasa.gov*

DRC-99-10

Data-Acquisition System Takes 8-Bit Samples at 1 GHz

There are numerous potential applications in high-speed sampling and processing of signals.

Goddard Space Flight Center, Greenbelt, Maryland

A unique data-acquisition system converts analog input voltages to 8-bit digital data at a rate as high as 10^9 samples per second (1 GHz), stores the data, and makes the data available for further processing. The system is compact, is highly resistant to ionizing radiation, consumes relatively little power, and is made from commercially available components. Designed for original use as part of a spaceborne laser altimeter, such data-acquisition systems could be adapted to potential terrestrial use as general-purpose high-speed analog-to-digital converters in electronic test equipment and scientific instruments, and as memory devices for storing data to be processed in digital signal-processing systems.

The major subsystems and functions of the system are as follows: The system includes an 8-bit, 1-GHz analog-to-digital converter (ADC), emitter-coupled logic (ECL) circuits to slow (as explained below) the data signals to 83.33 megasamples per second, programmable gate arrays that further slow the data signals for efficient writing, and a static random-access memory (SRAM) that stores the data. If the data are encoded (as explained below) then in making the stored data available for processing, the programmable gate arrays are also reused as decoders during readout from the SRAM.

The master clock signal for the system is a sinusoidal signal with a frequency of 2 GHz. This signal is processed through a 2:1 frequency divider to obtain a 1-GHz, 1/2-duty-cycle square wave, which serves as a timing signal for the ADC. In the ADC, the input signal that one seeks to process is digitized to 8 bits. The ADC internally demultiplexes the digital data signal into two 500-MHz ECL channels, each channel containing the 8 data bits plus a data-ready signal. ECL flip-flops and shift registers then slow the 500-MHz data signals from the two channels into 83 1/3-MHz signals in twelve channels.

The data signals in the twelve 83 1/3-MHz channels are converted from ECL to transistor/transistor logic (TTL) levels, then passed to programmable gate arrays. The gate arrays contain flip-flops that collect the data in groups of four bytes. The gate arrays also contain logic circuits that generate standard address, chip-selection, reading, and writing signals for storing the data in or reading data from the SRAM at a rate of 20.833 MHz. In addition, the gate arrays generate a signal that indicates when the SRAM is full.

Acquisition of data is enabled or disabled by a single digital input bit. When acquisition is not enabled, the gate arrays

collectively serve as a portal through which a digital processor can read data from, and write data to, the SRAM by use of the processor's own address, chip-selection, reading, and writing signals. The data can be Gray-coded or Gray-decoded during such reading or writing. The data path between this system and a digital processor is 32 bits wide; this feature makes it possible for a high-performance processor to gain access to four data samples per transaction.

This work was done by Kenneth W. Wagner of **Goddard Space Flight Center**. *Further information is contained in a TSP [see page 1].*
GSC-14176

Books and Reports

Evolvable Multiagent Approach to Spacecraft Communication

A paper presents the concept of a system for autonomous communication among multiple satellites and other spacecraft. The design of the system would be based on an evolvable architecture of multiple intelligent agents (that is, artificial-intelligence constructs implemented in software and hardware) that would communicate and cooperate with each other in performing such tasks as enabling each spacecraft to track the others, analyzing communication links, dynamically making and breaking links, and otherwise generally allocating communication resources. The evolvable-multiagent approach to design calls for the application of advanced concepts of artificial intelligence, the use of evolutionary algorithms to develop artificial-intelligence rules in response to changing circumstances, and hardware-evolving methods. The evolutionary features of the agents would render the system adaptive and increase its operational robustness. The paper discusses some of the problems to be addressed in constructing the system, describes an example of an evolvable system containing knowledge-based agents, and describes some hardware modules that could be used in building the system.

This work was done by Sanda Mandutianu of Caltech for **NASA's Jet Propulsion Laboratory**. *To obtain a copy of the paper, "An Evolvable Multi-Agent Approach to Satellite Communication Systems," see TSP's [page 1].*
NPO-20432

BLANK PAGE

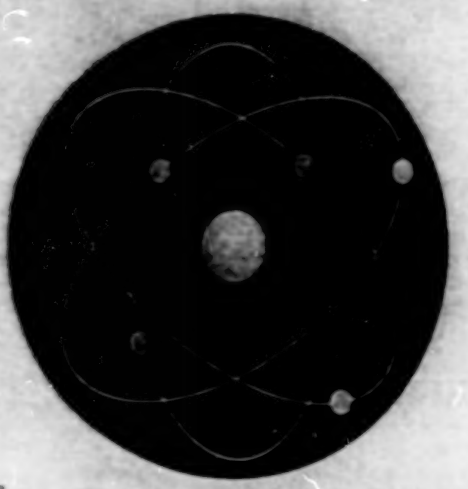

Physical Sciences

Hardware, Techniques, and Processes

27 Mathematical Modeling of Two-Phase Flow With Evaporation
28 Prismatic Phase Shifter
28 Temperature-Stable Magnetic Sector for Mass Spectrometer

Books and Reports

29 EPRI of Distributions of Free Radicals in Polyimide Samples

BLANK PAGE

Mathematical Modeling of Two-Phase Flow With Evaporation

Behaviors of evaporating liquid drops entrained in turbulent gas flows are simulated numerically.

NASA's Jet Propulsion Laboratory, Pasadena, California

A mathematical model constructed within a theoretical framework applicable to direct numerical simulation (DNS) predicts the behavior of evaporating liquid drops entrained in a turbulent shear layer.

In the model, liquid drops are assumed to be dispersed at low volume fraction (though not necessarily low mass fraction) in a carrier gas. All chemical species are assumed to be calorically perfect. Gravitation is neglected. It is assumed that values of the viscosity, thermal conductivity, and species diffusivity of the gas phase can be prescribed, independently of the local mixture fraction.

The compressible conservation equations for mass, momentum, and energy for the gas phase are formulated in an Eulerian reference frame and include terms to account for exchanges of mass, momentum, and energy with the drops. The drops are assumed spherical and their internal temperature is assumed uniform.

Each drop is tracked in a time-accurate manner in a Lagrangian reference frame; these equations include terms for the drag exerted on each drop by the surrounding flowing gas. Each drop is assumed to exchange heat with the gas phase through convection and conduction only, since this study is performed at low temperature. Evaporation is represented by the nonequilibrium Langmuir-Knudsen law. The model accounts for complete two-way phase coupling (both gas-to-liquid and liquid-to-gas) of mass, momentum, and energy based on a thermodynamically self-consistent specification of vapor enthalpy, internal energy, and latent heat of vaporization.

The model has been used to simulate the behavior of a three-dimensional, temporally developing, initially isothermal gas mixing layer formed by the merging of an airstream with a gas stream laden with hydrocarbon drops. Effects of the initial liquid-mass-loading ratio (*ML*), the initial Stokes number (St_0), the initial temperature of the drops, and the three-dimensionality of the flow on the evolution of the mixing layer were examined. The dominant parameter affecting the flow was found to be *ML* (for example, see figure). The laden stream was found to become saturated before evaporation was complete, at all but the smallest values of *ML*. Drops in the mixing layer were observed to be centrifuged out of regions of high vorticity and to migrate toward regions of high strain in the flow, with resultant formation of concentration streaks in spanwise braid regions wrapped around peripheries of secondary streamwise vortices. Persistent regions of positive and negative slip velocity and slip temperature were identified. Other characteristics examined included variances of liquid- and gas-phase velocities and relationships among gas-velocity, drop-number-density, and thermodynamic profiles. From considerations of first and second order statistics, a comprehensive picture of the mixing layer is described.

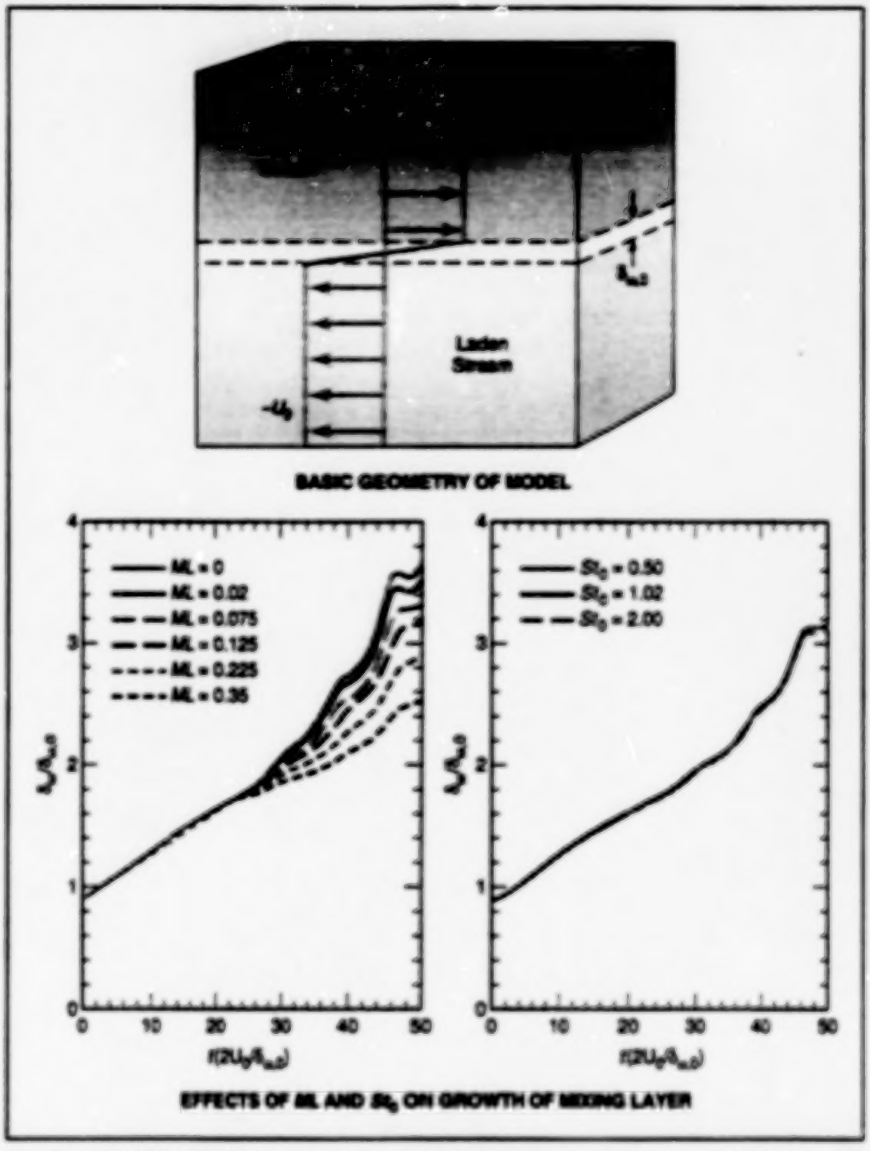

The Growth of the Mixing Layer was found to be increasingly attenuated with increasing *ML* in the range $0 \le ML \le 0.35$, but not appreciably affected by changes in St_0. On these plots, U_0 denotes the magnitude of each of the opposing free-stream velocities, *t* denotes time, $\delta_{\omega,0}$ represents a specified initial value of vorticity thickness, and δ_ω represents the vorticity thickness at any given time.

This work was done by Josette Bellan and Richard S. Miller of Caltech for **NASA's Jet Propulsion Laboratory**. *Further information is contained in a TSP [see page 1].*

NPO-20434

Prismatic Phase Shifter

Small phase changes can be obtained with relatively coarse mechanical adjustments.

Langley Research Center, Hampton, Virginia

The prismatic phase shifter is a novel device that can be used to control the phase of a coherent beam of light. Phase shifting is becoming an integral function of most modern interferometric systems. Phase shifting can be accomplished by use of any of a variety of older devices including moving mirrors, rotating quarter-wave plates, moving gratings, and Bragg cells, all of which have disadvantages. Surface losses and/or changes in polarization are induced by these various devices. In the case of a moving mirror, subwavelength translation can be difficult. Some of the other older devices produce lateral shifts of the beam.

The prismatic phase shifter introduces an easily controlled change of phase to a beam of light without the disadvantages of the older devices. This device consists of a prism mounted on a translation stage. The prism is placed in the beam oriented at the angle of minimum deviation. The orientation of the stage is chosen so that translation causes the prism to move along its plane of symmetry.

The figure shows the prism before (dashed) and after (solid) translation. Because of the symmetry of the configuration, the beam is not deviated or translated, and a phase shift is introduced to the beam. For decreasing apex angle, increased translation is needed to obtain a given phase shift. This effect is termed "optical leverage" and makes it possible to obtain small phase changes with relatively coarse mechanical adjustments.

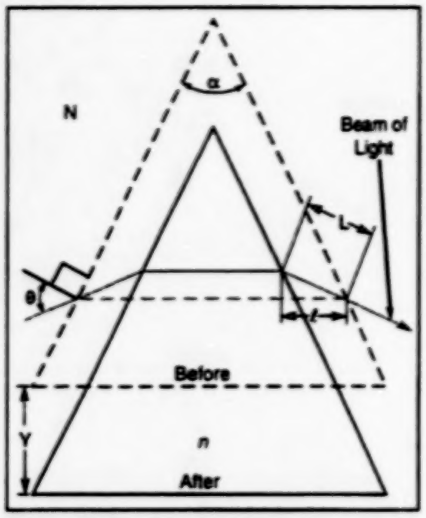

Phase Shift Is Introduced into the beam of light when the prism is moved along its plane of symmetry.

The change in effective optical-path distance, ΔOPD, is given by

$$\Delta OPD = 2\,(n\ell - NL)$$

where n and N are the indices of refraction of the prism and the surrounding medium, respectively; ℓ is half the difference between the old and new distances along the optical path inside the prism; and L is half the difference between the new and old distances along the optical path outside the prism. By the law of sines,

$$\frac{L}{\sin \alpha/2} = \frac{Y}{\cos \theta}$$

where Y is the translation distance, α is the apex angle of the prism, and θ is the angle of incidence for minimum deviation. This angle is given by

$$\theta = \arcsin\left[\frac{n^2 - n}{n - N}\sin \alpha/2\right]$$

Furthermore, ℓ is given by

$$\ell = \frac{Y \sin(\alpha/2)\cos(\theta - \alpha/2)}{\cos \theta}$$

Therefore, ΔOPD is given by

$$\Delta OPD = \frac{2Y \sin(\alpha/2)}{\cos \theta}\left[N - n\cos\left(\theta - \alpha/2\right)\right]$$

When this device is operated at Brewster's angle, it imposes no surface losses. The only requirement the prism material must satisfy is that it be transparent at the wavelength of interest and be of reasonable optical quality. Because translation of the prism to produce change of phase does not cause deviation or translation of the beam, the device can be used in a system in which strict alignment must be maintained.

This work was done by Brooks A. Childers of **Langley Research Center**. *Further information is contained in a TSP [see page 1].*

LAR-14637

Temperature-Stable Magnetic Sector for Mass Spectrometer

A temperature-sensitive magnetic shunt would compensate for a temperature-sensitive magnet.

NASA's Jet Propulsion Laboratory, Pasadena, California

A magnetic sector in a proposed miniature mass spectrometer would include (1) a permanent magnet made of a high-energy-product material, (2) a conventional ferromagnetic yoke, and (3) a small temperature-compensating magnetic shunt. In the absence of the temperature compensation, it would be necessary to restrict the operation of the miniature mass spectrometer to a controlled-temperature environment. With the temperature compensation, the instrument could be used to perform chemical analyses in a variety of laboratory, industrial, and field environments over a wide range of temperatures.

Alnico V	−0.02
Sm/Co	−0.04
Nd/B/Fe	−0.10

The **Temperature Coefficient of Remanent Flux Density** of the Nd/B/Fe alloy exceeds the corresponding coefficients of other permanent-magnet alloys.

The basic physical principle of a magnetic sector for a mass spectrometer dictates that mass of the permanent magnet be inversely proportional to the energy product of the permanent-magnet material. Therefore, a high-energy-product material is a key ingredient for miniaturization. The permanent-magnet material chosen for the proposed magnetic sector is an Nd/B/Fe alloy with an energy product of 45 to 50 MG·Oe (3.6 to 4.0 kJ/m^3). The aluminum/nickel/cobalt alloy (alnico V) previously used in mass spectrometers has an energy density of 5 to 6 MG·Oe (0.4 to 0.5 kJ/m^3). Thus, the use of the Nd/B/Fe alloy would enable a substantial reduction in the size of the permanent magnet.

Unfortunately, the Nd/B/Fe alloy has a negative temperature coefficient of rema-

nent flux density, and this coefficient is greater than that of alnico V and of another commonly used permanent-magnet alloy (see table). In the absence of temperature compensation, this would be problematic: The variation, with temperature, of the flux density in the magnet gap of the mass spectrometer would alter the mass calibration of the instrument. Thus, it would be necessary to perform frequent mass calibrations during operation. Alternatively, it would be necessary to maintain the instrument at constant temperature during operation; the means to do this would add to the size, weight, and power consumption of the instrument.

With respect to the magnetic circuit through the magnet, yoke, and gap, the magnetic shunt could be connected in parallel with either the permanent magnet or the gap. The shunt would be made of an Ni/Fe or Ni/Cr/Fe ferromagnetic alloy with a negative temperature coefficient of permeability. Thus, as the flux density of the permanent magnet decreased with increasing temperature (thereby tending to decrease the flux density in the gap), the reluctance of the shunt would increase (thereby tending to decrease the flux through the shunt and increase the flux through the gap). In other words, the needed effect would be to decrease the variation, with temperature, of the flux density in the gap. By suitable choice of the dimensions of the shunt, it should be possible to reduce the magnitude of the temperature coefficient of flux density in the gap to as little as 0.01 percent/°C over the temperature range from –40 to +20 °C.

This work was done by Mahadeva P. Sinha of Caltech for **NASA's Jet Propulsion Laboratory**. *Further information is contained in a TSP [see page 1].*

In accordance with Public Law 96-517, the contractor has elected to retain title to this invention. Inquiries concerning rights for its commercial use should be addressed to

Technology Reporting Office
JPL
Mail Stop 122-116
4800 Oak Grove Drive
Pasadena, CA 91109
(818) 354-2240

Refer to NPO-20332, volume and number of this NASA Tech Briefs *issue, and the page number.*

Books and Reports

EPRI of Distributions of Free Radicals in Polyimide Samples

A report describes experiments in which electron paramagnetic resonance imaging (EPRI) was used to determine one-dimensional spatial distributions of free radicals in two plate specimens of PMR-15 polyimide. One specimen had been postcured at a temperature of 315 °C in nitrogen, then thermally cycled 300 times between room temperature and 335 °C in air; the other specimen had been postcured at 316 °C in air, then further postcured at 371 °C in nitrogen, but not thermally cycled. EPRI of the thermally cycled specimen showed a higher concentration of free radicals in the surface layers than in the bulk. The shape of the EPR spectrum of the surface layer was found to remain the same as that of the bulk. EPRI of the non-thermally-cycled specimen showed no spatial variation in the concentration of free radicals. The authors interpret these EPRI results as suggesting that the thermo-oxidative degradation of PMR-15 polyimide involves free radicals present in the oxygen-rich surface layer.

This work was done by Mary Ann B. Meador of **Glenn Research Center**, *Myong K. Ahn of Indiana State University, and Sandra S. Eaton and Gareth R. Eaton of the University of Denver. To obtain a copy of the report, "Electron Paramagnetic Resonance Imaging of the Spatial Distribution of Free Radicals in PMR-15 Polyimide Resins," see TSP's [page 1].*

Inquiries concerning rights for the commercial use of this invention should be addressed to NASA Glenn Research Center, Commercial Technology Office, Attn: Steve Fedor, Mail Stop 4–8, 21000 Brookpark Road, Cleveland, Ohio 44135. Refer to LEW-16821.

BLANK PAGE

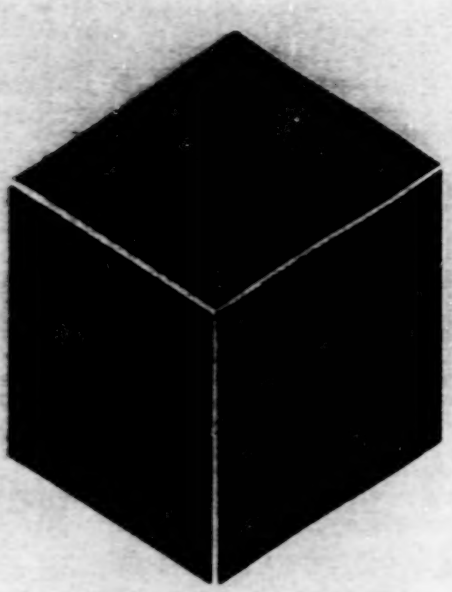

Materials

Hardware, Techniques, and Processes

33 Lightweight, Oxidation-Resistant $C_wSi_xO_yB_z$ Ceramics

33 Cheaper Polymeric Electrolyte Membranes for Fuel Cells

Books and Reports

34 Update on SiC-Fiber/[$MoSi_2$-Matrix/Si_3N_4 Particle] Composites

BLANK PAGE

Lightweight, Oxidation-Resistant $C_wSi_xO_yB_z$ Ceramics

Ceramic precursors are made by sol-gel impregnation of carbon preforms.

Ames Research Center, Moffett Field, California

Lightweight, monolithic ceramics that retain their shapes and strengths and resist oxidation at temperatures up to 1,200 °C have been invented. These ceramics are made of carbon, silicon, oxygen, and boron. These ceramics are made by (1) using a sol-gel process to infiltrate noncarbon ingredients into lightweight, porous carbon preforms; then (2) pyrolizing the infiltrated preforms.

A suitable carbon preform could be a piece of felt or boardstock, for example. Inasmuch as the finished monolithic ceramic article has the same size and shape as those of the preform, it is usually advantageous to start with a preform of the desired net size and shape.

In the sol-gel process used in this invention, the preform is immersed in a sol that comprises a mixture of silicon alkoxides and a borate ester (typically di- and tetrafunctional siloxanes and a boron alkoxide), then the sol is gelled in place. (Gelation comprises simultaneous hydrolysis and polymerization reactions.) The sol is prepared by mixing the siloxane and boron alkoxide reagents (see figure), preferably with an alcohol as a diluent. The alcohol prevents premature hydrolysis of the sol and ensures homogeneity of the sol.

Although the sol can be gelled by aging at ambient temperature or by heating, it is preferable to catalyze gelation by addition of an acid (e.g., HNO_3) or a base (e.g., NH_4OH) to the reaction mixture. Gelation of the catalyzed sol eventually occurs at ambient temperature, but it is further preferable to heat the impregnated preform gently to a temperature between 40 and 90 °C.

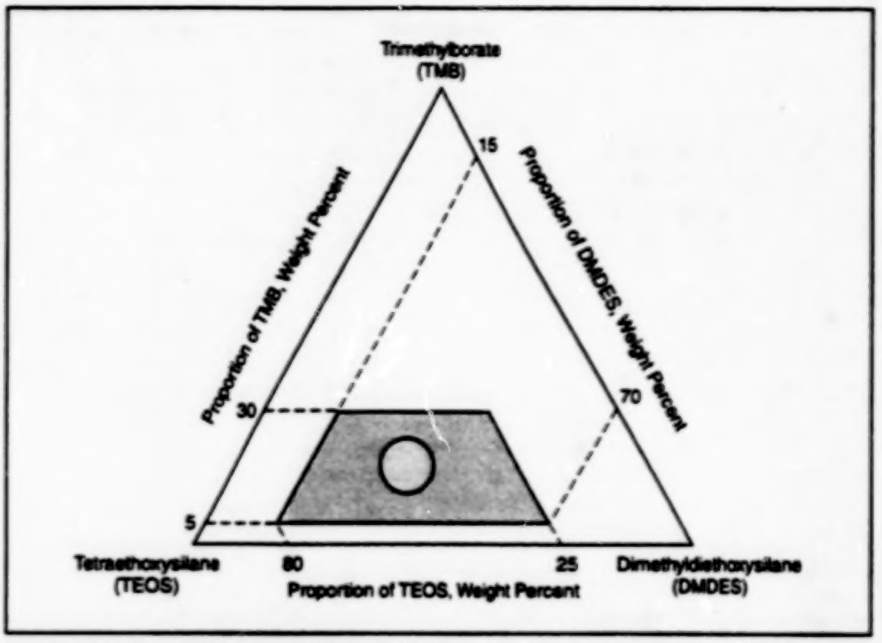

The Trapezoid on This Ternary Diagram encloses the range of proportions of three typical ingredients that can be used to make sols according to this invention. The range of optimum proportions is enclosed by the circle.

After gelation, the impregnated preform is removed from the gel and any surplus gel adhering to the preform is wiped off. The impregnated preform is then dried to form a ceramic precursor; preferably, the drying is done in a vacuum oven overnight at a temperature between 70 and 100 °C to ensure that all volatiles are removed before the pyrolysis step described next.

The dried, impregnated preform is heated in an inert gas (e.g., argon) or in a vacuum, preferably at a temperature between 900 and 1,200 °C. During this heating process, the carbon of the preform enters into pyrolysis reactions with the dried gel and thereby becomes part of the ceramic.

This work was done by Daniel B. Leiser, Ming-ta Hsu, and Timothy S. Chen of **Ames Research Center**. *Further information is contained in a TSP [see page 1].*

This invention has been patented by NASA (U.S. Patent No. 5,618,766). Inquiries concerning nonexclusive or exclusive license for its commercial development should be addressed to the Patent Counsel, Ames Research Center [see page 1]. Refer to ARC-12096.

Cheaper Polymeric Electrolyte Membranes for Fuel Cells

In addition to costing less, these membranes resist methanol crossover.

NASA's Jet Propulsion Laboratory, Pasadena, California

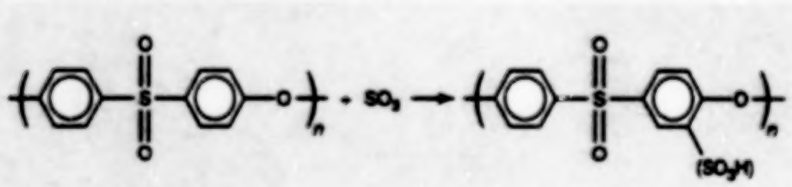

Sulfonated Poly(Phenylether Sulfone) Is Synthesized by sulfonation of a sulfonated poly(phenylether sulfone) base polymer with sulfur trioxide in the presence of methylene chloride.

Proton-conductive (solid-electrolyte) membranes made from sulfonated poly(phenylether sulfone), plus membrane/electrode assemblies containing these membranes, have been developed for use in methanol fuel cells. These membranes offer two important advantages over traditional fuel-cell membranes made of a commercial perfluorosulfonic acid-based ion-exchange polymer:

1. Whereas the traditional membranes cost about \$900/m^2 (as of 1997), the present membranes are expected to cost between \$5/m^2 and \$10/m^2.
2. The traditional membranes are somewhat permeable by methanol; crossover by methanol is a parasitic process that reduces fuel-cell efficiency. The present membranes offer greater resistance to

methanol crossover.

The figure illustrates the synthesis of sulfonated poly(phenylether sulfone). Degrees of sulfonation can be controlled to obtain polymers of various equivalent molecular weights. Any of these polymers or a mixture of them can be dissolved in dimethyl formamide (DMF) to form a casting "dope." Other ingredients can be added to the mixture to modify the properties of the membranes to be formed subsequently. To form a membrane, one casts the dope on a suitable surface in air, by use of a casting apparatus with a doctor blade.

Of the membranes of this kind tested thus far, the best one was made from a 75-percent portion of sulfonated poly(phenylether sulfone) of 620 daltons equivalent molecular weight plus a 25-percent portion of the unsulfonated base polymer. The incorporation of the unsulfonated base polymer adds strength and reduces crossover, relative to the pure sulfonated polymer. The casting dope formed by dissolving this mixture of polymers in DMF is not a true solution and, instead, appears to be more like an emulsion.

Casting twice has been found to be essential to formation of a stable dope and casting of a useful membrane. On first casting, the dope separates into what are presumed to be ionomeric (sulfonated) and inert (unsulfonated) phases. The polymer as thus cast is redissolved in DMF to form a new dope. Upon casting from the new dope, phase separation does not occur; the precise physicochemical mechanism responsible for this phenomenon has not been established, though it has been conjectured to be a consequence of absorption of a small amount of water from the air immediately after the first casting.

The fabrication of a membrane/electrode assembly includes, among other things, hot-pressing a membrane between carbon papers that have been coated with electrode-catalyst/liquid-ionomer mixtures, with the coated sides in contact with the membrane. To achieve adequate adhesion between the anode and the membrane, it is necessary to modify the anode-side membrane surface, prior to hot pressing, by rubbing it with a small amount of carbon-supported anode catalyst.

The electrical characteristics of fuel cells containing membrane/electrode assemblies of this type are similar to those of similarly dimensioned fuel cells containing traditional membrane/electrode assemblies. However, the present membrane/electrode assemblies operate with less methanol crossover; for example, the membrane/electrode assembly made with the best membrane exhibited about as much methanol crossover as would be expected of a membrane/electrode assembly containing a traditional membrane of three times the thickness.

This work was done by Shiao-Ping Yen, Andrew Kindler, Andre Yavrouian, and Gerald Halpert of Caltech for **NASA's Jet Propulsion Laboratory**. *Further information is contained in a TSP [see page 1].*

In accordance with Public Law 96-517, the contractor has elected to retain title to this invention. Inquiries concerning rights for its commercial use should be addressed to

Technology Reporting Office
JPL
Mail Stop 122-116
4800 Oak Grove Drive
Pasadena, CA 91109
(818) 354-2240

Refer to NPO-20251, volume and number of this NASA Tech Briefs *issue, and the page number.*

Books and Reports

Update on SiC-Fiber/[$MoSi_2$-Matrix/Si_3N_4 Particle] Composites

A report presents updated information on the developments described in "$MoSi_2$-Based Composite Materials for Aircraft Engines" (LEW-16617), *NASA Tech Briefs*, Vol. 22, No. 9 (September 1998), page 62. To recapitulate: Hybrid composites of (1) SiC-based fibers within (2) matrices that are, themselves, composites of $MoSi_2$ containing 30 to 50 volume percent of Si_3N_4 particles are candidate high-temperature-resistant materials for use in advanced aircraft engines. The addition of the Si_3N_4 particles (1) results in the formation of an Si_2ON_2 protective scale that increases resistance to low-temperature accelerated oxidation, which otherwise causes catastrophic "pest failure" of $MoSi_2$; (2) increases high-temperature creep strength to almost 10^5 times that of neat $MoSi_2$; (3) doubles room-temperature toughness; and (4) decreases the coefficient of thermal expansion to such an extent as to eliminate matrix cracking in the presence of SiC-based fiber reinforcement, even after thermal cycling. The inclusion of the SiC-based fiber reinforcement increases room-temperature fracture toughness by a factor of about 7 and impact resistance by a factor of about 5. A specimen of a composite of this type coated with BN and Si_3N_4 exhibited no surface or matrix cracking even after it was exposed to a jet-fuel flame in a gas turbine engine.

This work was done by Mohan G. Hebsur of Ohio Aerospace Institute for **Glenn Research Center**. *To obtain a copy of the report, "Development and Characterization of SiC/$MoSi_2$-Si_3N_4(p) Hybrid Composites," see TSP's [page 1].*

Inquiries concerning rights for the commercial use of this invention should be addressed to NASA Glenn Research Center, Commercial Technology Office, Attn: Steve Fedor, Mail Stop 4–8, 21000 Brookpark Road, Cleveland, Ohio 44135. Refer to LEW-16884.

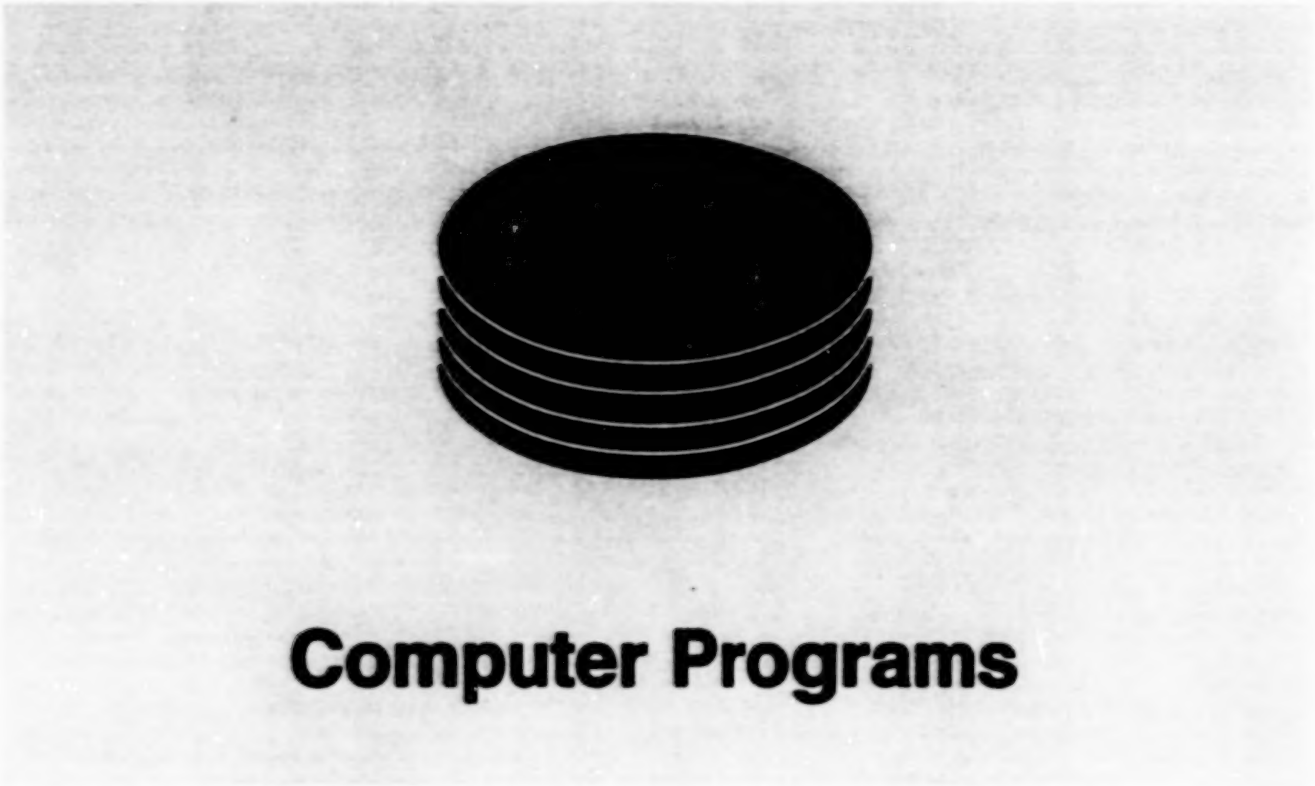

Computer Programs

Mechanics

37 On-Line System Provides Accurate Ephemeris and Related Data

Mathematics and Information Sciences

37 Program Generates Maps From IFSAR Data
37 Software for Planning and Execution in an Autonomous System
37 Software Library for Parallel Adaptive Mesh Refinement

BLANK PAGE

Mechanics

On-Line System Provides Accurate Ephemeris and Related Data

The Horizons On-Line Ephemeris and Data System ("Horizons" for short) is a computer program that provides data on the locations, motions, and dynamical parameters of solar-system objects, including the Sun, nine planets, 61 natural satellites, more than 16,000 comets and asteroids, and several dynamical points. Designed to be the reference standard for solar-system dynamical astronomy, Horizons is more comprehensive than any ephemeris or almanac published before in paper or software, and its data are the most accurate available from any source. Designed for use by professionals, Horizons can also be used by others; it is maintained on a server computer and is accessible to the public via the Internet. A user is given the best information available at the time of use. Horizons operates in multiple coordinate systems, includes a many-body integrator that propagates asteroid and comet orbits, and provides a search capability for identification of astronomical objects from parameters specified by the user.

This work was done by Jon D. Giorgini and Donald Yeomans of Caltech for **NASA's Jet Propulsion Laboratory**. *Further information should be requested via the Internet from http://ssd.jpl.nasa.gov/horizons.html.*

This software is available for commercial licensing. Please contact Don Hart of the California Institute of Technology at (818) 393-3425. Refer to NPO-20416.

Mathematics and Information Sciences

Program Generates Maps From IFSAR Data

A computer program provides for automated generation of maps from data acquired via C-band interferometric synthetic-aperture radar (IFSAR). The program reads in height, radar-brightness, and correlation data generated by IFSAR processors and computes a series of image features to be used in classifying terrain. Correlations between IFSAR channels are used to estimate new terrain-classification parameters. Classification is accomplished by use of a Bayesian classifier and is followed by spatial editing of terrain classes. Next, various additional layers of data (pertaining to IFSAR height error, shaded relief, drainage, and mountains) are computed and the data are projected into the universal transverse Mercator coordinate system. The results of the foregoing process are then turned into cartographic products with the help of commercially available software.

This program was written by Ernesto Rodriguez, Thierry Michel, Jan Martin, and Bijan Houshmand of Caltech for **NASA's Jet Propulsion Laboratory**. *For further information, see TSP's [page 1].*
NPO-20325

Software for Planning and Execution in an Autonomous System

A software system for planning and execution of actions by an autonomous spacecraft engaged in scientific exploration has been developed to satisfy requirements to (1) maintain positive resource margins and avoid short-sighted decisions in order to achieve long-term scientific and engineering goals while (2) responding quickly to changing circumstances in order to take advantage of unexpected opportunities for gathering scientific data or to recover from equipment malfunctions or adverse environmental events. The software is based on an integrated planning-and-execution architecture that supports continuous modification of a current working plan in response to continuously arriving updated information on the activities, resources, and the state of the spacecraft and its environment. After each update, its effects are propagated through current projections, which are limited in order to avoid unnecessary work. When conflicts arise in the plan as modified pursuant to the updates, iterative repair and local-search techniques are used to resolve the conflicts.

This program was written by Steve Chien, Robert Sherwood, Gregg Rabideau, Russell Knight, and Andre Stechert of Caltech for **NASA's Jet Propulsion Laboratory**. *For further information, see TSP's [page 1].*

This software is available for commercial licensing. Please contact Don Hart of the California Institute of Technology at (818) 393-3425. Refer to NPO-20590.

Software Library for Parallel Adaptive Mesh Refinement

A software library has been developed for use in parallel adaptive refinement of unstructured (irregular) meshes and grids in parallel scientific and engineering computing. This library can be used in finite-difference, finite-volume, and finite-element application programs that use two-dimensional triangular meshes or three-dimensional tetrahedral meshes. The library contains a suite of well designed and efficiently implemented modules that perform common operations in a parallel-adaptive-mesh-refinement (PAMR) process. These operations include (1) quality control during a successive PAMR process, typically guided by a local-error-estimate algorithm; and (2) parallel dynamic load-balancing of an adaptive mesh. The library was implemented in Fortran 90 and uses a message-passing-interface (MPI) library to support modularity, efficiency, and portability. The library is currently available on a Cray T3E computer at the Goddard Space Flight Center, and is being ported to a cluster of personal computers (a Beowulf-class system).

This program was written by John Z. Lou and Charles D. Norton of Caltech for **NASA's Jet Propulsion Laboratory**. *For further information, see TSP's [page 1].*
NPO-20583

BLANK PAGE

Mechanics

Hardware, Techniques, and Processes

41 Shrouds Would Catch Debris From Disintegrating Machines

42 Vibratory Accelerometer and Gyroscope

Books and Reports

42 Computational Test Cases for a Rectangular Supercritical Wing

BLANK PAGE

Shrouds Would Catch Debris From Disintegrating Machines

Kinetic energy of debris would be transformed into controlled breakage of shroud materials.

Lyndon B. Johnson Space Center, Houston, Texas

Kinetic-energy-absorbing shrouds have been proposed to protect nearby persons and equipment against high-speed debris ejected by disintegrating machines. Examples of machines that could eject high-speed debris include turbines and gyroscopes. The shrouds would be laminated composites of several materials that would be designed to transform the kinetic energy of impinging debris into controlled, progressive breakage of the materials, so that the debris would become trapped harmlessly within the shrouds.

Each shroud (see figure) would contain two layers of overlapping longitudinal metal strips surrounded by circular straps made of a strong webbing material (e.g., made from aromatic polyamide fibers). Before wrapping around the cylinder defined by the metal strips, each strap would have a circumference greater than that of the cylinder. Each strap would be sized to fit snugly on the cylinder in the following way: At numerous equidistant points around the circumference, the strap would be doubled to form loops that would be sewn together with a stitch that would rip apart by an applied load slightly below the breaking strength of the webbing itself. Thus, the straps would be capable of absorbing energy in a controlled manner by progressive ripping of the stitches.

All the looped straps thus fabricated would be assembled side by side over the cylinder of metal strips. The sewn loops would be folded to lie circumferentially against the outer surface. Depending on the specific design, another subassembly comprising another two layers of metal strips and another layer of straps with sewn loops could be formed around the previous one. The entire assembly would then be encapsulated in a rigid, low-strength foam, thereby forming a unitary energy-absorbing cylinder that would be mounted around the rotating component that posed a disintegration hazard.

Upon disintegration of the rotating component, fragments of the component would first impinge on the metal strips, forcing them into the energy-absorbing straps. The force in each affected strap would increase until it reached the ripping load, at which point the stitches in the loops would begin to come apart. During this process, the foam would break, allowing the straps to react to the force. The total energy absorbed in this way would be approximately equal to the product of the ripping force and the displacement of each strap. If the shroud were to contain multiple layers (in contradistinction to a single layer) of energy-absorbing straps, the overall radial displacement could be limited to a smaller value because each layer of straps would absorb a fraction of the total energy.

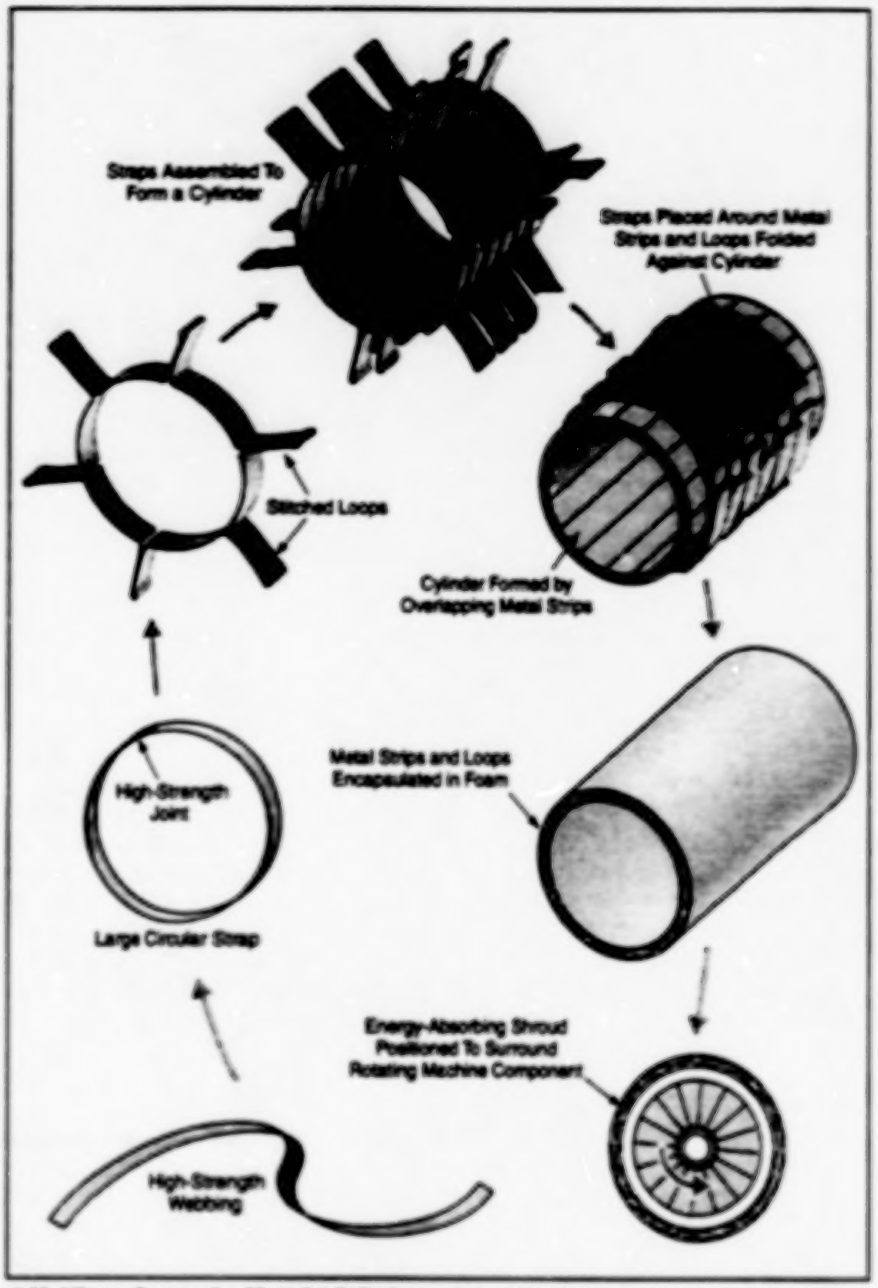
Straps Assembled To Form a Cylinder
Straps Placed Around Metal Strips and Loops Folded Against Cylinder
Stitched Loops
Cylinder Formed by Overlapping Metal Strips
Metal Strips and Loops Encapsulated in Foam
High-Strength Joint
Large Circular Strap
Energy-Absorbing Shroud Positioned To Surround Rotating Machine Component
High-Strength Webbing

A Multilayer Composite-Material Cylinder would be fabricated, then placed around a rotating machine component to catch debris from disintegration of the component.

This work was done by William C. Schneider of **Johnson Space Center**. *Further information is contained in a TSP [see page 1].*

This invention is owned by NASA, and a patent application has been filed. Inquiries concerning nonexclusive or exclusive license for its commercial development should be addressed to the Patent Counsel, Johnson Space Center, (281) 483-0837. Refer to MSC-22823.

Vibratory Accelerometer and Gyroscope

Subtle effects related to vibrational degeneracy and mass imbalance are exploited.

NASA's Jet Propulsion Laboratory, Pasadena, California

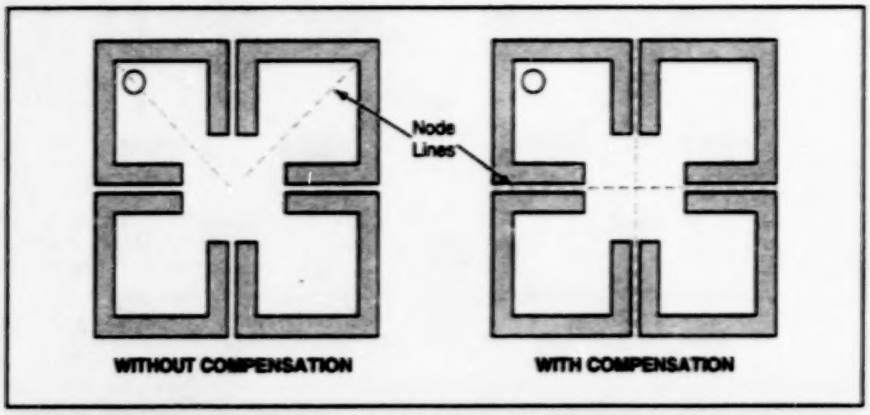

A Planar Resonator that resembles a four-leaf clover is symmetrical except for a small mass imbalance at the location of the circle. The node lines of the degenerate vibrational modes lie along one or the other set of dashed lines, depending on whether or not the mass unbalance is compensated electrostatically.

A device that measures both translational acceleration and rotation exploits the dynamics of a vibratory structure that resembles a clover leaf. This device is related to other vibratory accelerometers and vibratory gyroscopes in which vibrations in suitably shaped structures are excited electrostatically and measured either capacitively or piezoresistively. The basic principle of this device could also be applied to a different structure, provided that, like the clover-leaf structure, it vibrates in substantially degenerate modes and provided further that it has a small mass imbalance.

The figure depicts the clover-leaf structure in the present device. This structure vibrates in two degenerate modes. A small mass imbalance defines the shape of the modes in that it causes the node lines of the vibrational pattern to lie along (1) a line that runs through the geometric center of the structure and the location of the mass imbalance and (2) a line perpendicular to the aforementioned line. In the presence of a nominal constant (e.g., zero) rotation or constant translational acceleration, it is possible to rotate the node lines to make them coincide with the Cartesian axes of symmetry of the structure; this is accomplished by applying an electrostatic force of such a magnitude as to contribute a negative spring-stiffness component that compensates for the mass imbalance.

The vibrational dynamics are such that a change in the translational acceleration perturbs the compensation, causing the node lines to rotate back toward alignment with the mass unbalance. In operation in an open-loop mode, the rotation of the node lines can be deduced from the amplitude and phase relationships among the outputs of the capacitive vibration sensors. Alternatively, the device can be operated in a closed-loop mode in which the signals are processed into feedback control signals that adjust the electrostatic force to keep the node lines from rotating; in this case, the feedback control signal serves as an indication of the angular velocity or translational acceleration. It is possible to measure rotation and translational acceleration simultaneously and separately because the translation- and rotation-related capacitive-sensor outputs come out in quadrature with each other.

This work was done by Roman Gutierrez and Tony K. Tang of Caltech for ***NASA's Jet Propulsion Laboratory****. Further information is contained in a TSP [see page 1].*

This invention is owned by NASA, and a patent application has been filed. Inquiries concerning nonexclusive or exclusive license for its commercial development should be addressed to the Patent Counsel, NASA Resident Office–JPL [see page 1]. Refer to NPO-20620.

Books and Reports

Computational Test Cases for a Rectangular Supercritical Wing

A report describes wind-tunnel experiments on a rectangular supercritical wing and presents test cases that have been selected from the archived sets of experimental data for comparison with computational fluid dynamics (CFD) predictions. In the experiments, the wing was driven in pitching oscillations at frequencies below the lowest natural vibration frequency of the wing. The data obtained in the experiments included the static pressures and the in-phase and quadrature components (with phases referenced to the pitching motion) of unsteady pressures at a number of points on the upper and lower wing surfaces. Mach numbers from 0.27 to 0.90 and static angles of attack of 0°, 2°, and 4° are included. From several hundred compiled data points, 27 static and 36 pitching-oscillation cases were chosen for computational test cases to illustrate trends with mach number, angle of attack, and reduced frequency ($\omega c_r/2V_\infty$, where $\omega = 2\pi \times$ frequency of pitching oscillation, c_r is the wing root chord, and V_∞ is the free-stream speed), and angle of attack. The data for these cases are presented in graphs and tables.

This work was done by Robert M. Bennett and Charlotte E. Walker of ***Langley Research Center****. To obtain a copy of the report, see TSP's [page 1].*
L-17830

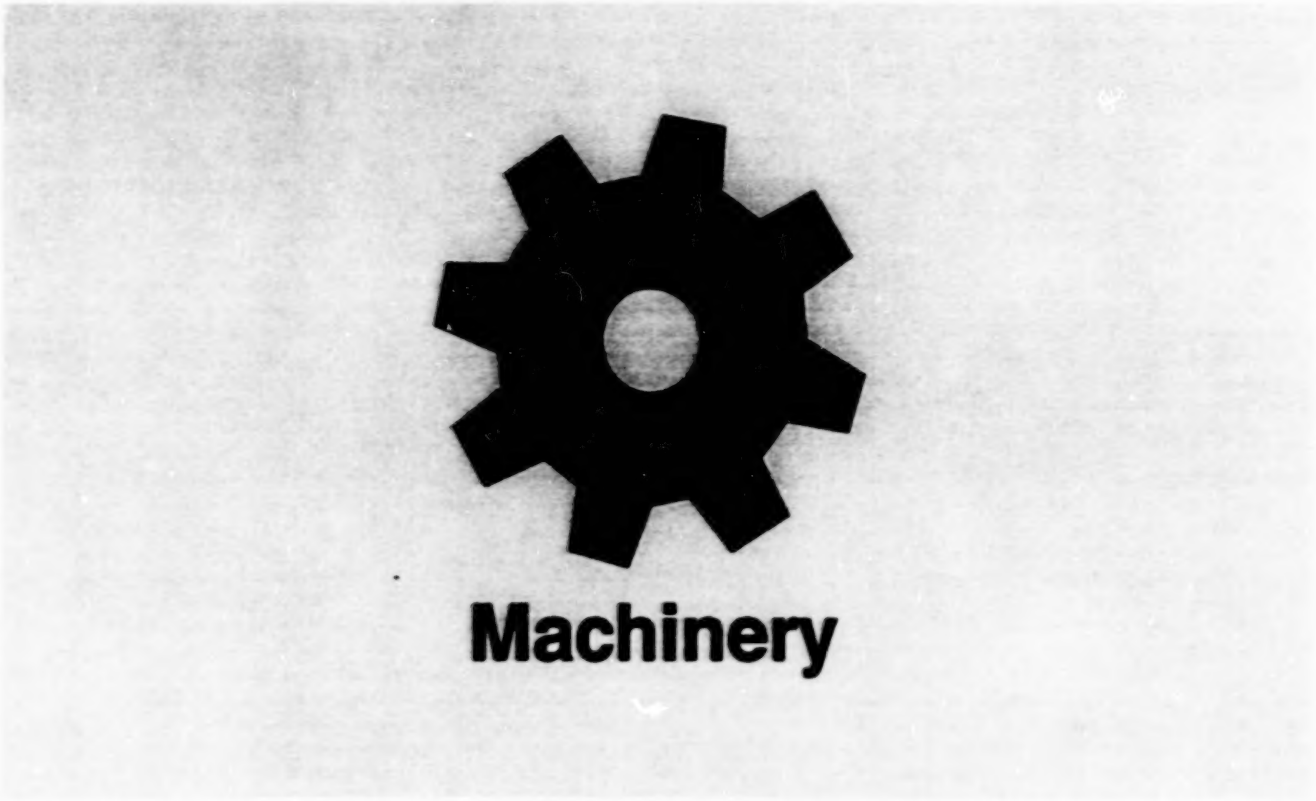

Machinery

Hardware, Techniques, and Processes

45 Device Assists Actuation of a Joint in a Pressure Suit
46 Model X-33 Subscale Flight Research Program
46 Biomorphic Robot With Distributed Power

Books and Reports

47 Modifications of the Ventricular Assist Device

BLANK PAGE

Device Assists Actuation of a Joint in a Pressure Suit

The full range of motion can be restored when human power is partially or fully lost.

Lyndon B. Johnson Space Center, Houston, Texas

An electromechanical device implements a unique method of actuating a fabric joint in an inflatable structure — in particular, the joint in an astronaut's pressure suit. The method is based on the principle that power from an external source can be applied to a non-constant-volume joint in a pressure suit to actuate the joint without human force. Actuation of the joint by power from an external power source enables the astronaut to conserve energy for tasks that require more dexterity.

The design of the device is relatively simple. The figure shows the device installed as part of a pressure-suit glove, but the device can be applied to any similar inflatable structure. A drive shaft made of flexible cable or rigid segments, driven via internal and external ball hex couplings, is positioned to intersect a palm bar, which is on the palm side of the glove at the metacarpal joint. The drive shaft goes through several drive hubs, rotating within mountings that include a band and a spacer block. Retracting panels are wrapped around the drive shaft. When torque is applied via the drive shaft, the panels wind around the shaft; this causes the panels to pull on anchor points, thereby retracting the joint (closing the palm). Thus, by use of this device, the wearer can flex the metacarpal joint without using any muscle power.

An input sensor positioned either inside or outside the pressure suit exhibits changing electrical resistance in response to control movement of the wearer's hand. The sensor output signal is fed as input to an external control system that drives an electric motor. The motor, in turn, drives the flexible shaft and a gear drive unit. A feedback sensor is incorporated into the gear drive unit for additional response.

This device is potentially applicable beyond the U. S. Space Program. Devices like this one could easily be applied to other pressure-suit joints, or could be used on inflatable mobility joints for individuals who suffer from joint diseases and have partially or fully lost the use of the affected joints. The device could restore the full range of motion to a diseased joint or optimize the motility of a healthy joint being used under extreme conditions like zero gravity. In a case of therapeutic use on an inflated mobility joint to restore movement to a nonfunctioning limb, the input sensor could be placed on another limb or digit that is functional. Clearly, this device is a significant advance in the field of bionics and of potential benefit to both public and private sectors.

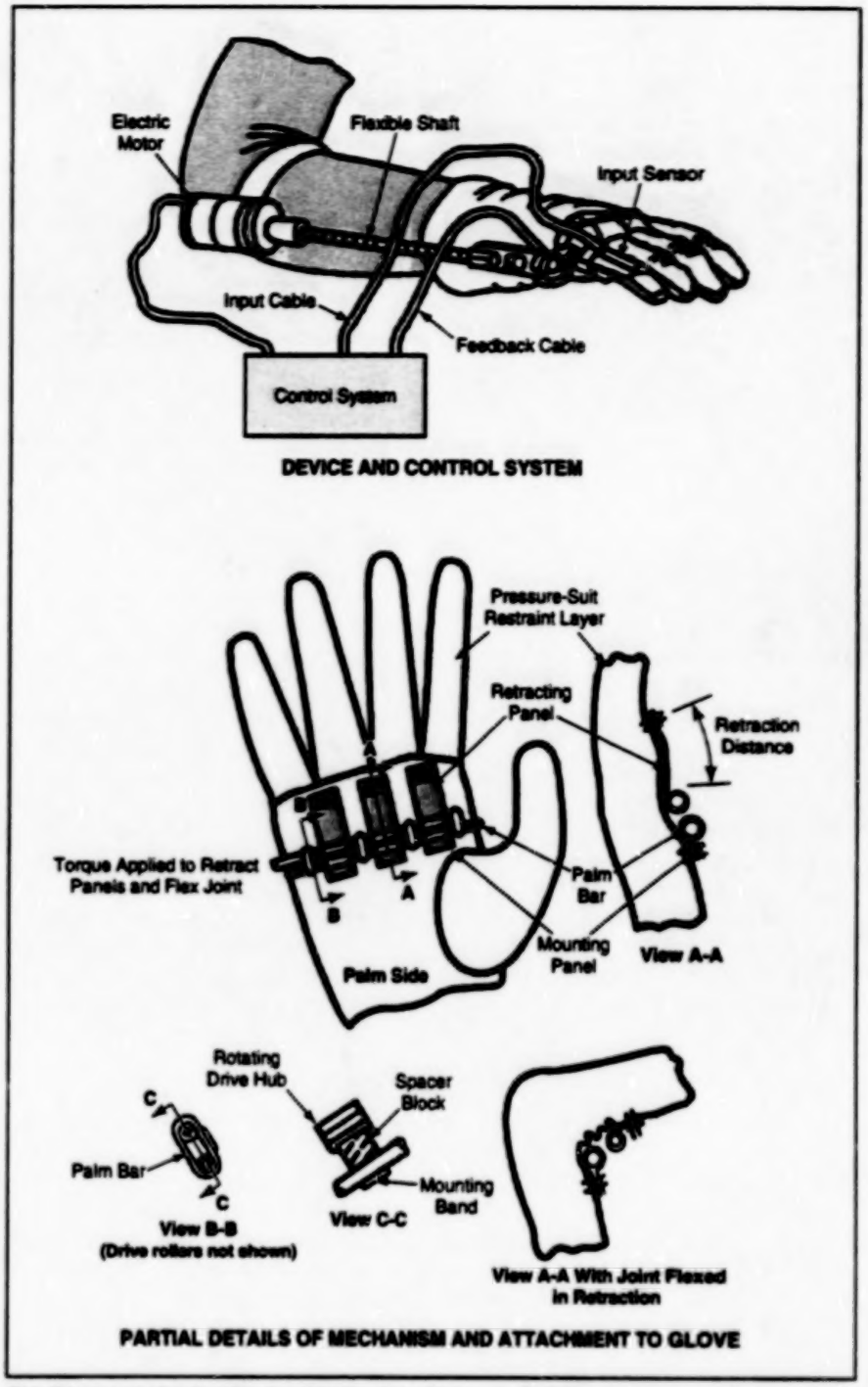

This Electromechanical Device Attached to a Pressure-Suit Glove uses power from an external source to assist the wearer in flexing the metacarpal (palm) joint. In response to the wearer's hand motion, the input sensor generates an input to the control system.

This work was done by Daniel G. Cencer of **Johnson Space Center**. *No further documentation is available.*

This invention is owned by NASA, and a patent application has been filed. Inquiries concerning nonexclusive or exclusive license for its commercial development should be addressed to Patent Counsel, Johnson Space Center, (281) 483-0837. Refer to MSC-22797.

Model X-33 Subscale Flight Research Program

This program advances the development of the X-33 and the art of model flight testing.

Dryden Flight Research Center, Edwards, California

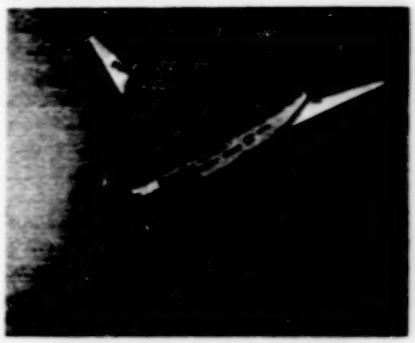

MODEL WITH TOP OFF TO SHOW INSTRUMENTATION AND SOME STRUCTURAL DETAILS

MODEL IN FLIGHT, ABOUT TO TOUCH DOWN

The X-33 Model is instrumented for flight tests in which it is launched at altitude, then descends and lands on the ground.

A program of flight testing of an instrumented subscale model of the X-33 aerospace vehicle is underway. The objectives of this program are the following:

- Successful flight of a model of the X-33;
- Development of a small, lightweight, instrumentation system suitable for model research;
- Determination of limited X-33 aerodynamic characteristics from flight data; and
- Quantification of how well parameter-estimation techniques perform when applied to data acquired by use of the lightweight instrumentation system on a model of this type.

The program is justified by the fact that model flight-testing often highlights unforeseen characteristics, and by the potential for applying the flight-test techniques and instrumentation developed in this program to flight testing of other subscale, lightly loaded models of aerospace vehicles.

The X-33 model (see figure) is 4 ft (1.2 m) long and was fabricated in the landing-gear-down configuration. The model has been flown 29 times to date, and 16 channels of instrumentation were in use during the last 20 flights. The model weighs 8 lb (3.6 kg) empty and 11 lb (5 kg) with instrumentation. The 3-lb (1.4-kg) instrumentation system, developed specifically for the X-33 model, includes a power supply, sensors, and related wiring. The model is visually controlled from the ground and has no stability augmentation. Because of its limited performance, stability, and control, the X-33 configuration is a challenging one to fly and land.

A typical flight operation starts with the launching of the X-33 model from a larger, powered model at an altitude of 1,000 ft (305 m). There is time to perform one flight-data maneuver prior to setup for landing. The model is back on the ground about 25 seconds after launch. The flight data are then downloaded into a laptop computer. The flights thus far have been used to mature the hardware, establish the best combination of vehicle trim and center of gravity, and gather limited flight data.

Some of the flight data gathered thus far have been analyzed. Several maneuvers have been successfully analyzed by use of parameter-estimation techniques. Moments of inertia were recently experimentally determined. A detailed calibration of air-data parameters will soon follow, and further analyses of flight data will be performed once the calibration is complete. There are plans to evaluate additional lightweight sensors.

This work was done by Alex G. Sim and Jim Murray of **Dryden Flight Research Center** *and Tony Frackowiak of Analytical Services and Materials, Inc. Further information is contained in a TSP [see page 1].*

DRC-99-22

Biomorphic Robot With Distributed Power

The major advantages would be simplicity and reliability.

NASA's Jet Propulsion Laboratory, Pasadena, California

The biomorphic robot with distributed power (BIROD) is a prototype of a class of robots that will contain simple, reliable distributed actuators that will consume power from local sources — a design concept inspired in part by biological actuators like muscles in limbs. The BIROD concept stands in contrast to the traditional machine-design concepts of (1) central (therefore vulnerable) sources of power and (2) distribution of power through complex (therefore troublesome) linkages that include gears, pulleys, levers, and other mechanisms. The BIROD concept is potentially applicable not only to robots but also to systems as diverse as home appliances, automobiles, and spacecraft.

At the time of reporting the information for this article, the BIROD had been designed, assembled, and the initial motor movements were demonstrated. The initial design calls for the use of electrical power to actuate muscle wires. (A muscle wire is made of a shape-memory alloy. By sending a sufficient electric current along the wire, one can heat the wire above its transition temperature, causing it to change length. When the current is turned off, the wire cools, returning to its original length.)

With further development, BIROD designs might evolve toward greater degrees of biomorphism. For example, actuators might be made to derive energy from locally stored chemicals that could be recharged; in this aspect, the BIROD chemical/energy cycle would be reminiscent of the adenosine diphosphate/adenosine triphosphate (ADP/ATP) cycle in biological systems. Going even further toward biomorphism, BIRODs might even be made capable of repairing themselves.

This work was done by Kumar Ramohalli of Caltech for **NASA's Jet Propulsion Laboratory**. *Further information is contained in a TSP [see page 1].*

NPO-20606

Modifications of the Ventricular Assist Device

A report discusses some modifications of the ventricular assist device (VAD), which was described in "Small Implantable Pump Would Assist Circulation of Blood" (MSC-22424) *NASA Tech Briefs*, Vol. 20, No. 7 (July 1996), page 86. The VAD is a surgically implantable, miniature rotary pump designed to assist in pulmonary or systemic circulation of blood. The modifications, guided by computational simulations of blood flow in the pump, were directed partly toward reducing stagnant flow, backflow, and unsteady flow in order to reduce shear stresses and thereby reduce damage to blood cells and thereby, further, reduce clotting. The modifications were also directed toward increasing pumping efficiency. The report describes a series of seven designs, six of which incorporate various modifications of a baseline design. The modifications include changes in the shapes and dimensions of a hub, impeller blades, and gaps. The report notes that tests have shown that the modifications do not completely eliminate clotting, but are effective in reducing clotting and improving the performance of the pump.

This work was done by Bernard J. Rosenbaum of **Johnson Space Center**, *Dochan Kwak of Ames Research Center, Robert J. Benkowski of the Baylor College of Medicine, and Kris Catin of MCAT Institute. To obtain a copy of the report, "Ventricular Assist Device," see TSP's [page 1].*

This invention is owned by NASA, and a patent application has been filed. Inquiries concerning nonexclusive or exclusive license for its commercial development should be addressed to the Patent Counsel, Johnson Space Center, (281) 483-0837. Refer to MSC-22822.

BLANK PAGE

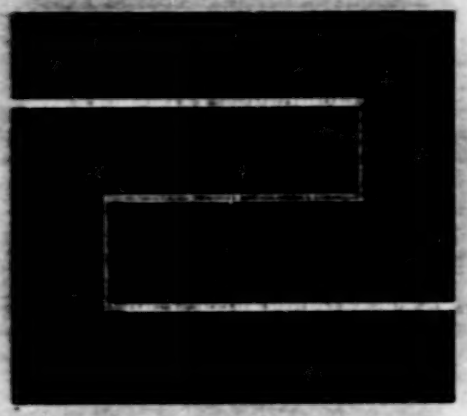

Fabrication Technology

Hardware, Techniques, and Processes

51 Modified Wire Tie

51 Heated Weights for Adhesive Bonding

BLANK PAGE

Modified Wire Tie

The modified tie is scored to facilitate separation of excess material.

Langley Research Center, Hampton, Virginia

A common self-locking plastic wire tie has been modified (see figure) to enable the installer to snap off excess tie material after installation, without need for a cutting tool and without creating a potentially hazardous sharp end. A typical unmodified wire tie of this type is available in any of a variety of sizes and is made of nylon or another plastic. When the unmodified tie is tightened around a bundle of wires or other object, the excess tie material (the material that protrudes from a unitary locking mechanism at one end of the tie) must be cut off flush with the locking mechanism by use of a special tool. Often, an installer does not possess such a tool or cannot use the tool because of space limitations. Consequently, the installer often resorts to cutting the excess material with a wire cutter, which can leave a dangerously sharp protruding end.

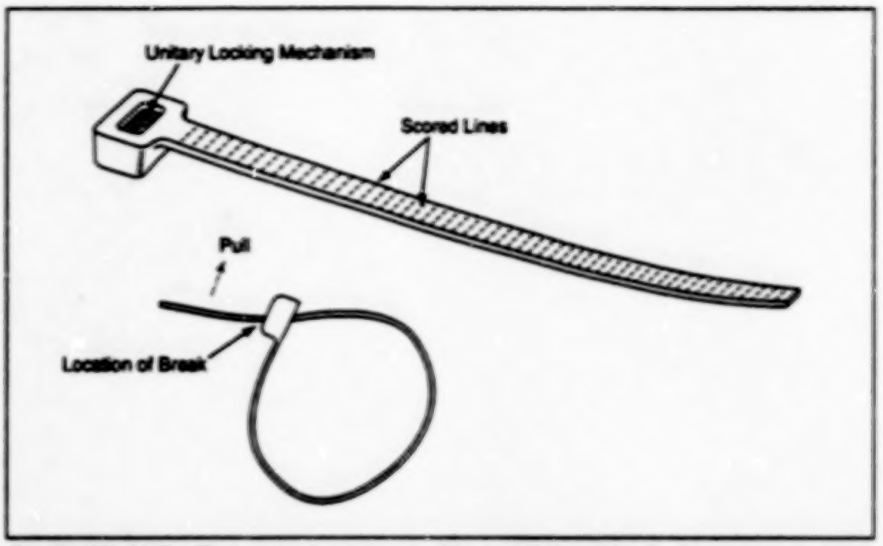

The Modified Wire Tie is scored at intervals. After installation of the tie, the excess tie material is snapped off at the score closest to the unitary locking mechanism.

The modification consists in scoring the underside of the tie at intervals of about 1/16 in. (1.6 mm) along its length. After the tie is tightened in place, the excess material can be pulled back and snapped off at the scored line nearest the unitary locking mechanism, leaving a short, nearly flush end.

This work was done by Arthur R. Hayhurst of **Langley Research Center**. *No further documentation is available.*
LAR-15103

Heated Weights for Adhesive Bonding

The risk of overheating is eliminated, without need for monitoring.

Goddard Space Flight Center, Greenbelt, Maryland

Heated weights have been found to be useful in adhesive bonding of clips, doublers, and other small parts to lightweight structures and structural components (e.g., face-sheet/honeycomb-core sandwich panels). The heated weights provide both the heat needed to accelerate curing of the adhesive and the force needed to clamp the bonded parts together until the cure is complete.

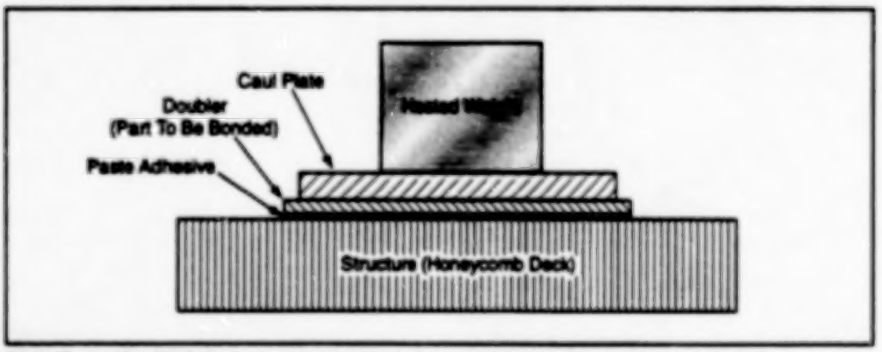

Heat From the Weight is coupled through the caul plate to the part to be bonded.

The heated-weight technique was developed in support of the Top Hat Balloon Project, wherein the technique is used to accelerate the cure of a paste adhesive for bonding inserts. The technique makes it possible to shorten the bonding process from two days to one. The technique can afford similar benefits in the fabrication of structural components for aircraft and spacecraft.

Local heating for accelerating the cure of an adhesive becomes necessary when the structure in question is too large to put in an oven or when heat-sensitive equipment has already been installed on the structure. Therefore, local heating has commonly been accomplished by use of heat lamps or electric heating blankets, and clamping forces have been applied by weights, clamps, or vacuum bags. Heat lamps or electric blankets must be monitored closely to ensure that maximum allowable curing temperatures are not exceeded, and heat-sensitive equipment must be removed or protected. In contrast, the heated-weight technique does not require close monitoring or special preparations to protect heat-sensitive equipment, yet it inherently ensures that the maximum allowable curing temperature for a given bond is not exceeded and that heat is applied only in the vicinity of the bond.

In preparation for bonding by the heated-weight technique, a caul plate is machined from a highly thermally conductive material (e.g., aluminum or copper) to the profile of the small part to be bonded to a structure. In an oven, a suitable weight is preheated to a temperature equal to or less than the maximum

allowable curing temperature for the adhesive used in the bond. The caul plate is placed on the part to be bonded, and the heated weight is placed on top of the caul plate (see figure). The caul plate distributes the weight and heat evenly over the part. If additional heating time is needed to complete the cure, then additional weights can be heated and used to replace the previous heated weight(s).

This work was done by James Parker and David Puckett of **Goddard Space Flight Center**. *No further documentation is available.*
GSC-13866

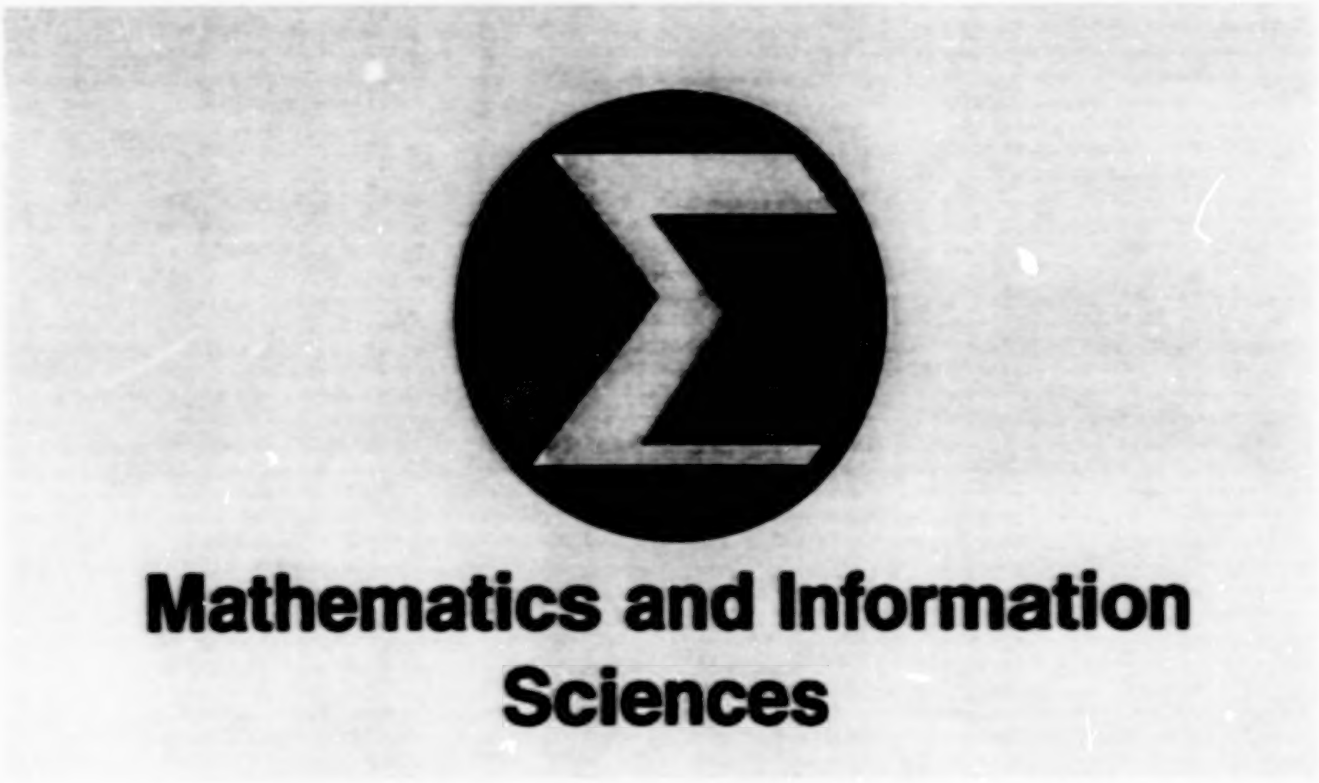

Mathematics and Information Sciences

Hardware, Techniques, and Processes

55 Software for Managing Distributed Real-Time Data

56 Proper Orthogonal Decomposition in Optimal Control of Fluids

Books and Reports

57 Strategies for Optimal Placement of Sensors and Actuators

57 Configuration Management of Software for Designing HSCT4.0

BLANK PAGE

Software for Managing Distributed Real-Time Data

Collaborative computing and acquisition of data are combined.

Dryden Flight Research Center, Edwards, California

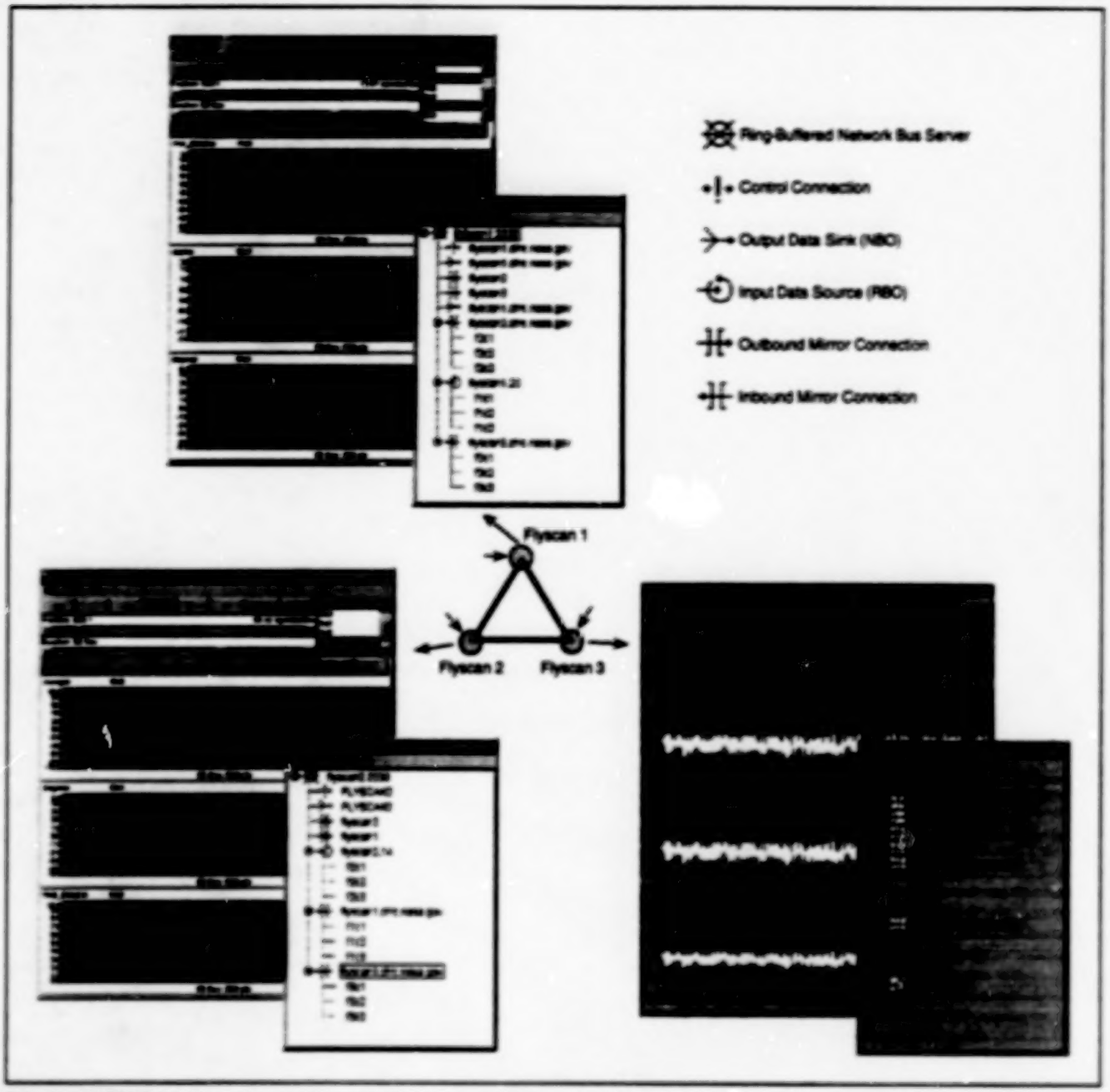

This Simple RBNB Configuration could be regarded as representing a potential baseline architecture for such enterprise-scale applications as merging data streams from multiple sources or merging sensor data with data of other types (e.g., processed results, multimedia, or any other associated information).

An all-software data server has been invented to enable any set of connected application programs to create or gain access to live data streams. (As used here, "connected" signifies running on either the same computer or on different computers and communicating via the Internet, an intranet, or another network.) In combination with seamless archiving and retrieval of historical data, the invention offers new opportunities for distributed computing.

The Ring-Buffered Network Bus (RBNB™) is an all-Java-software data server that makes the network appear to be, simultaneously, a shared-memory server, a data-acquisition system, and a distributed data base. It extends the Transmission Control Protocol/Internet Protocol (TCP/IP) sockets subprotocol by incorporating a frame/channel management scheme and the ability to split and merge data streams on a channel-by-channel basis. Because streams can be routed or mirrored to other RBNB servers, configurations can readily be scaled for reasons of performance, redundancy, and security.

Core RBNB architectural components are software objects that manage streams (frames) of data. A frame is a time-stamped

unit that contains one or more channels of data, each channel containing one or more data elements. Successive frames can contain fixed or variable sets of channels.

An essential part of the RBNB is a ring buffer object (RBO). For input of data from a particular source, an RBO acts as both a data server and an archive manager. An RBO manages multiple frames in a ring buffer that effects a seamless transition from RAM to disk. The "ring" of an RBO is a circular buffer that, if necessary, writes over oldest data. Users can add descriptive header information to support a variety of downstream data-management and -processing schemes.

For output of data, a network bus object (NBO) manages requests for data and sends the selected channels. The output data stream is a new stream that contains frame and channel header information from one or more originating RBO sources. The user or the data sink can request individual frames and time slices, or can request that the data be streamed continuously for higher performance.

The core RBNB routes data as structured blocks of bytes; by design, the RBNB does not respond to or alter the intrinsic data format. This feature provides optimal flexibility and efficiency, but leaves the job of "understanding" data to the associated sources and sinks. When it is preferable to increase compatibility among otherwise incompatible sources and sinks, "plug-in" format converters can be invoked. A format converter (FC) processes the source data, creating the desired stream for the data sink. Examples of format conversion include simple units conversion, decompression, decryption, demultiplexing, or any other operation on the data. Channels of information created by FCs are indistinguishable from other channel types. Format conversions are independent processes that are executed locally or on remote computers.

The figure shows a simple RBNB configuration that involves three computers on a network (flyscan 1, flyscan 2, and flyscan 3). On each computer, an RBNB server accepts requests from data sources and data sinks. On each computer, a source process prepares three signals and sends them to an RBO in the local RBNB server. Mirrors are set up from each RBO to two remote RBNB servers, providing local access to all nine channels from any of the three servers. In the figure, a graphical view of connections is provided via a management utility called "rbnbAdmin." Access to the data is demonstrated on each computer via a strip-chart utility program, called "rbnbPlot," also running on each computer.

The performance of the all-Java data server is impressive. Aggregate throughput on modern personal computers and entry-level workstations exceeds 12 MB/s to random-access memory (RAM) and 8 MB/s to disk. Performance continues to improve as computer technology and Java both mature.

This work was done by Lawrence C. Freudinger of **Dryden Flight Research Center** *and Matthew J. Miller, Ian A. Brown, and William R. Baschnagel of Creare, Inc. The Small Business Innovation Research (SBIR) contractor has elected to retain rights in the invention and a patent is pending. The contractor will introduce the RBNB in 1999 as a commercial product. Additional information is available on line at http://outlet.creare.com/rbnb. Inquiries should be addressed to the SBIR Technology Transfer Office, NASA Dryden Flight Research Center; telephone (805) 258 3720. DRC-96-34*

Proper Orthogonal Decomposition in Optimal Control of Fluids

Suitably formulated reduced-order mathematical models can be satisfactory approximations for purposes of control.

Langley Research Center, Hampton, Virginia

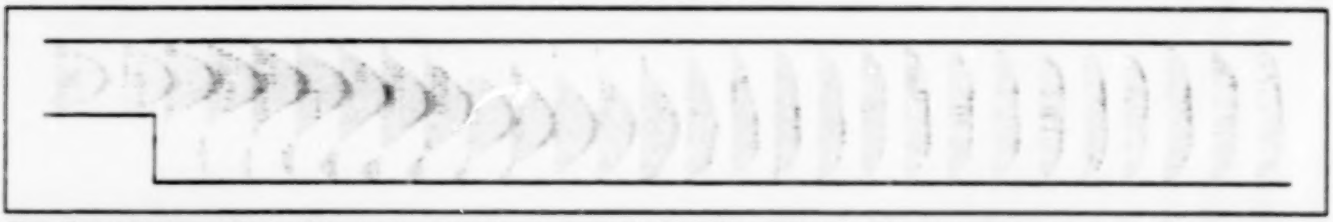

Flow Over a Backward-Facing Step in a two-dimensional channel at a Reynolds number of 1,000 was chosen as a test case. The arrows shown here represent velocity vectors at selected positions. Computational simulations have shown that recirculation (represented by the reversal of arrows) immediately downstream of the step can be reduced by use of optimal blowing control according to the methodology described in the text.

A methodology proposed for actively controlling flows involves the use of proper orthogonal decomposition (POD) to derive computational models of reduced order. The methodology could be particularly useful for controlling flows of gases and liquids in real time.

The need for reduced-order modeling arises because of the inherent complexity of the computations for solving the full Navier-Stokes equations for the dynamics of fluids. One can reduce the time and cost of computation by use of reduced-order models. The problem is to derive suitable reduced-order models that approximate the essential dynamics well enough for purposes of control. The present POD-based methodology provides a systematic and optimal way to derive reduced-order models of relatively high accuracy while maintaining well-conditioned matrices in a matrix-vector form of the dynamical equations ("system matrices" for short). The methodology may not be effective in all cases and must be applied with care. In those cases in which it is effective, it can provide adequate control performance at significantly reduced computational cost.

The conventional approach to the discretization of the Navier-Stokes equations or other nonlinear partial differential equations by use of a finite-difference, finite-element, spectral method involves the use of basis functions (e.g., trigonometric functions, Legendre polynomials, or piecewise polynomials) that are mathematically convenient but that have very little connection with either the underlying physics of a specific case or the corresponding partial differential equations. In contrast, POD involves the use of basis functions generated from experiments or from numerical solutions of the partial differential equations. More specifically, it involves the extraction of an optimal set of basis functions (perhaps containing only a few basis functions) from a computational or experimental data base, by use of an eigenvalue analysis. Then by means of Galerkin projection, a solution is calculated as a linear combination of basis functions from the

optimal set. This solution is the desired reduced-order model solution.

In a test case, the methodology was applied to a two-dimensional flow in a channel that includes a backward-facing step. At high Reynolds numbers, the flow separates and recirculation appears (see figure). The problem was formulated as one of blowing of fluid on part of the step surface to reduce the recirculation and thereby reduce the length of reattachment. Computational simulations with as few as 9 POD modes showed that optimal blowing control could effectively eliminate separation and significantly reduce the size of the recirculation bubble and the reattachment length.

This work was done by S. S. Ravindran of **Langley Research Center**. *Further information is contained in a TSP [see page 1].*
L-17846

Books and Reports

Strategies for Optimal Placement of Sensors and Actuators

A paper presents a survey of sensor- and actuator-placement problems from various applications that involve a wide range of engineering disciplines. "Smart" structures that contain sensors (e.g., microphones or strain sensors) and actuators (e.g., loudspeakers or piezoelectric actuators) can be used, for example, to control the shapes of airfoils or to suppress noise or structural vibrations. In designing a "smart" structure, one faces the problem of placing limited numbers of sensors and actuators to maximize some measure of performance; typically, the locations must be selected from a large set of candidate locations. Of the problems of this type surveyed in the paper, most were solved by use of combinatorial-optimization algorithms. Three example applications from NASA Langley Research Center are presented: (1) active structural acoustic control involving actuators attached to an aircraft fuselage to control noise in the passenger compartment, (2) optimum placement of sensors for system identification and control of aeroelastic structures, and (3) positioning a minimum number of actuators that would be used to vary the shape of an airplane wing for three-axis flight control.

This work was done by Sharon L. Padula of **Langley Research Center** *and Rex K. Kincaid of the College of William and Mary. To obtain a copy of the paper, "Optimization Strategies for Sensor and Actuator Placement," see TSP's [page 1].*
L-17839

Configuration Management of Software for Designing HSCT4.0

A report discusses the development of a highly complex system of distributed-computing, multidisciplinary design-optimization software, called "CJOpt," for use in research on model 4 of the High-Speed Civil Transport (HSCT) airplane (HSCT4.0). The emphasis in the report is on the application of formal software configuration management (SCM) to ensure the integrity of, and the traceability of changes in, the optimization software. The report begins with an introduction that briefly describes the evolution of HSCT-design software along with the sequence of HSCT models leading up to HSCT4.0. Next, the general concepts of SCM and the implementation of these concepts within the HSCT4.0/CJOpt project are described. The report concludes with a discussion of the experiences in the application of SCM to the HSCT4.0/CJOpt project and some of the lessons learned from these experiences.

This work was done by James C. Townsend, Andrea O. Salas, and M. Patricia Schuler of **Langley Research Center**. *To obtain a copy of the report, "Configuration Management of an Optimization Application in a Research Environment," see TSP's [page 1].*
L-17868

END

02-18-00